

Discovery of Nonlinear Dynamics with Automated Basis Function Generation

Mohammad Amin Basiri^{1,*} and Charles Nicholson^{1,2,†}

¹*Data Science and Analytics Institute,*

University of Oklahoma, Norman, OK, USA

²*School of Industrial and Systems Engineering,*

University of Oklahoma, Norman, OK, USA

(Dated: May 12, 2026)

arXiv:2605.09696v1 [cs.LG] 10 May 2026

Abstract

Discovering governing equations from observational data remains a fundamental challenge in scientific modeling, particularly when the underlying mathematical structure is unknown. Traditional sparse identification methods like SINDY excel at discovering parsimonious models but require researchers to specify candidate basis functions *a priori*, a limitation that often leads to model failure when critical terms are omitted or when systems exhibit unconventional dynamics. Purely symbolic regression approaches offer unlimited flexibility but struggle with noise sensitivity and frequently produce overly complex, unstable equations. We present AUTOSINDY, a hybrid *Discovery-then-Solve* framework that combines the exploratory power of symbolic regression with the robust sparsity-promoting capabilities of SINDY. Our method operates in three stages: (1) PYSR-based symbolic regression discovers candidate functional forms from bootstrapped data chunks; (2) a curation pipeline decomposes, expands, and filters these expressions using collinearity analysis to construct a minimal yet comprehensive library; and (3) SINDY identifies sparse governing equations from this custom-tailored library. Extensive experiments across canonical nonlinear systems (oscillatory, chaotic, etc.) demonstrate that AUTOSINDY consistently recovers ground-truth equations even under high observational noise, achieving a ground-truth recovery rate of 92.8% across all trials. Compared with standard SINDY using enriched libraries and standalone symbolic regression, AUTOSINDY achieves higher predictive accuracy, superior generalization to unseen trajectories, and substantially lower symbolic complexity. These results show that AUTOSINDY successfully identifies correct governing terms without prior domain knowledge, effectively automating the feature-engineering bottleneck in system identification and offering a scalable pathway for discovering complex dynamics in biological and physical systems where the mathematical form is unknown.

I. INTRODUCTION

The discovery of governing mathematical equations from observational data is one of the deepest aspirations of the scientific method. From Johannes Kepler, who inferred the laws of planetary motion from decades of astronomical records, to Newton formulating the clas-

* ma.basiri@ou.edu

† cnicholson@ou.edu

sical mathematical description of universal gravitation and the laws of motion [1], scientists have long sought compact, interpretable models that reveal the mechanistic structure beneath experimental observations. Today, this ambition is being transformed and accelerated by the rise of scientific machine learning. Artificial intelligence and data-driven modeling are now deeply integrated into the entire scientific workflow, from automated hypothesis generation and experimental design to the discovery of novel physical laws directly from high-dimensional, multivariate time-series data [2, 3]. The governing equations of dynamical systems occupy a privileged position in this landscape: they are the ultimate compressed representation of a physical or biological process, encoding causality, generalizability, and mechanistic interpretability in a form that no black-box model can provide. Recovering these equations from data has profound implications across domains where first-principles derivations are intractable, such as fluid mechanics [4], plasma physics [5], climate models [6], neuroscience [7], and systems biology [8]. As both the volume of scientific data and the computational power available for analysis continue to grow, the need for principled, automated, and assumption-free methods for equation discovery has never been more urgent.

Two dominant and complementary paradigms have emerged for data-driven discovery of governing equations: sparse regression-based identification and symbolic regression. The Sparse Identification of Nonlinear Dynamics (SINDY) framework, introduced by Brunton, Proctor, and Kutz [9], formulates equation discovery as a sparse regression problem over a user-specified library of candidate functions. Assuming that most dynamical systems can be described by only a few active terms from a large dictionary of possible nonlinearities, SINDY applies sequentially thresholded least squares (STLSQ) to identify the minimal subset of library functions that best fits the measured time derivatives of the state. This elegant formulation produces interpretable, parsimonious models and requires substantially less data than neural-network-based approaches. Its generalization to partial differential equations (PDEs) via PDE-FIND [10] further broadened its scope, and the open-source PYSINDY ecosystem [11, 12] has consolidated a rich family of extensions, including SINDY with control inputs [13], implicit formulations for rational nonlinearities [14], and autoencoder-based coordinate discovery [15]. Subsequent innovations have markedly improved robustness and model selection: Sparse Relaxed Regularized Regression (SR3) [16] handles correlated library terms through a convex relaxation; weak-form SINDY [17] bypasses noisy derivative estimation by integrating against test functions; SINDY-AIC [18] applies the Akaike information

criterion (AIC) to automatically select the most parsimonious model; and E-SINDY [19] leverages bootstrap aggregating (bagging) to identify probabilistic models robust to limited data and high noise. In parallel, symbolic regression offers a fundamentally different and complementary approach: rather than selecting terms from a pre-built dictionary, it searches the space of mathematical expressions using evolutionary algorithms. Following the foundational work of Koza [20] and the landmark Eureqa platform of Schmidt and Lipson [21], modern tools such as PYSR [22] have established symbolic regression as a practical method for recovering governing equations across physical, biological, and epidemiological systems [23].

However, despite these significant advances, critical limitations prevent either paradigm from serving as a fully general-purpose solution for automated equation discovery. The central bottleneck of SINDY-based methods is their dependence on a user-specified candidate library: the correct governing terms must be anticipated and explicitly included prior to any regression. If a critical basis function is omitted, whether due to unconventional dynamics, unexpected nonlinearities, or genuine domain ignorance, the method fails to recover the true model regardless of the downstream optimizer [8, 24]. Enriching the library with an exhaustive set of candidate terms partially addresses omission errors but introduces severe multicollinearity among features, destabilizes sparse regression, and inflates coefficient uncertainty [16, 19]. A major remaining challenge is therefore to construct libraries that are simultaneously expressive enough to contain the true governing terms and compact enough to avoid redundancy and collinearity, a requirement that cannot be satisfied by any fixed or generic library in the absence of domain knowledge. Symbolic regression addresses the library problem directly, but this flexibility comes at a steep price: the combinatorial nature of expression tree search renders it computationally intensive, highly sensitive to measurement noise, and prone to producing overfitted expressions that are numerically unstable when integrated as differential equations [22, 23]. Moreover, because symbolic regression methods optimize each state variable independently, they struggle to enforce the coupled structure of multi-dimensional dynamical systems [8]. The broader challenge, which is automatically constructing a minimal, physics-appropriate function library from raw data without any prior knowledge of the system’s mathematical form, remains an open and critical problem in scientific machine learning.

In this work, we present AUTOSINDY, a hybrid *Discovery-then-Solve* framework designed

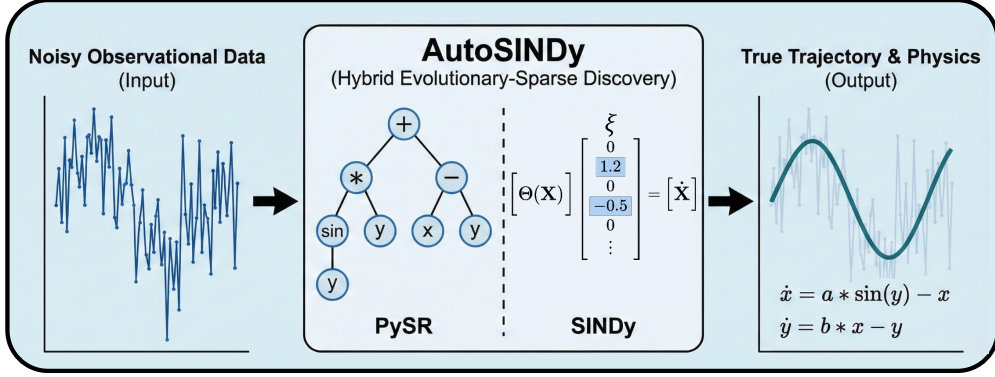


FIG. 1. Conceptual overview of AUTOSINDY. Noisy observational data (left) enters a hybrid evolutionary-sparse discovery engine (centre): PySR searches the symbolic space via expression-tree evolution, producing a set of candidate functional forms that is then filtered by SINDY’s sparse regression. The output (right) is a concise, closed-form governing equation that faithfully reconstructs the underlying physics.

to directly bridge this gap. The key insight is a structural decomposition of the equation discovery problem: symbolic regression, applied locally to short bootstrapped data subsets, need not solve the complete discovery problem, it needs only surface plausible candidate functional forms efficiently. These candidates are then systematically curated and handed to SINDY for precise, sparse coefficient identification. This separation of *structure discovery* (what functional forms might appear) from *sparse selection* (which terms are active and with what coefficients) allows each component to operate in the regime where it excels. AUTOSINDY thus recovers the expressive power of symbolic regression while retaining the interpretability, efficiency, and robustness of SINDY, without requiring any domain knowledge about the system’s mathematical form. Figure 1 provides a high-level illustration of this pipeline.

The primary contributions of this work are as follows.

1. **Automated, assumption-free library generation.** We propose a PySR-based discovery engine [22] that operates over bootstrapped data chunks, mining candidate functional forms through evolutionary optimization with no prior specification of the mathematical structure. This directly addresses the library design bottleneck that limits all fixed-library SINDY variants [9, 18].
2. **A principled symbolic curation pipeline.** We introduce a three-stage curation

mechanism that decomposes raw symbolic expressions into atomic basis functions, applies configurable expansion strategies (severe, gentle, or hybrid), and prunes multicollinear features via variance inflation factor (VIF) analysis with a simplicity bias. This pipeline transforms unstructured genetic algorithm output into a clean, non-redundant linear basis amenable to robust sparse regression.

3. **Ensemble-based sparse identification with hard-cutoff thresholding.** We integrate the curated library with the SINDY suite of optimizers, such as STLSQ or SR3 [16], and a bootstrap ensemble approach with configurable inclusion-probability thresholding, extending the E-SINDY framework [19]. Terms appearing in less than a user-specified fraction of bootstrap models are discarded, providing strong noise rejection without sacrificing interpretability.
4. **Systematic benchmarking against strong baselines.** We evaluate AUTOSINDY on canonical nonlinear systems spanning oscillatory, limit-cycle, and chaotic regimes under varying noise levels, comparing against standard SINDY with enriched polynomial-Fourier libraries and standalone symbolic regression. AUTOSINDY consistently recovers ground-truth governing equations, achieving higher predictive accuracy, superior generalization to unseen trajectories, and substantially lower symbolic complexity than either baseline.

The remainder of this paper is organized as follows. Section II reviews related work on sparse identification, symbolic regression, and hybrid equation discovery methods. Section III presents the AUTOSINDY framework in detail. Section IV describes the experimental setup and evaluation metrics. Section V reports results and comparative analysis. Section VI discusses implications, limitations, and future directions. Section VII concludes.

II. RELATED WORK

Data-driven equation discovery lies at the intersection of sparse optimization, evolutionary computation, and scientific machine learning. We survey the most relevant lines of work, organized by methodology and proximity to the AUTOSINDY framework.

A. Sparse Identification of Nonlinear Dynamics

The SINDY algorithm [9] established the modern framework for sparse, library-based equation discovery. Given state measurements and their time derivatives, SINDY assembles a matrix of candidate nonlinear functions, typically polynomials and trigonometric terms, and recovers the governing equations as the sparse solution to an overdetermined regression problem using STLSQ. The extension PDE-FIND [10] applied this principle to partial differential equations, enabling the recovery of spatiotemporal governing laws such as the Navier-Stokes and Kuramoto-Sivashinsky equations from data. The PYSINDY software package [11, 12] has become the standard implementation platform, providing modular support for library construction, optimizer selection, and integration with automatic differentiation tools.

Building on this infrastructure, a rich family of SINDY variants has addressed distinct limitations of the original formulation. The SINDY-control extension [13] incorporates external control signals, enabling discovery of actuated dynamics from input-output data. Implicit-SINDY [14] extends the framework to rational function nonlinearities through cross-multiplication. Autoencoder-SINDY [15] jointly learns a coordinate transformation into a parsimonious latent space and discovers the sparse governing equations within it.

Noise robustness has been a persistent focus. The weak-form SINDY approach [17] reformulates the regression problem in an integral form, multiplying both sides by smooth test functions and integrating over time windows, effectively averaging out noise and eliminating the need for direct derivative computation. E-SINDY (Ensemble-SINDY) [19] takes a complementary statistical approach, applying bagging to SINDY: an ensemble of models is identified from subsets of the data, inclusion probabilities are computed for each candidate library term, and terms with low inclusion probabilities are thresholded, providing uncertainty quantification and robustness in the low-data, high-noise limit.

Model selection has also received sustained attention. SINDY-AIC [18] integrates the AIC into the SINDY pipeline, ranking candidate models by their balance of goodness-of-fit and parametric complexity. The variant of Dong *et al.* [24] further incorporates group sparsity to identify coefficient-dependent PDEs and introduces a formal treatment of noise distribution estimation. SR3 [16] replaces STLSQ with a convex relaxation that decouples coefficient shrinkage and thresholding, improving performance in the presence of highly

correlated library features. Probabilistic approaches, including sparse Bayesian formulations with spike-and-slab and horseshoe priors [25], provide full posterior distributions over model coefficients at the cost of higher computational burden.

Across all of these advances, the fundamental limitation remains unchanged: the quality of the identified model is bounded above by the quality of the user-specified candidate library. This library design problem is the primary motivation for AUTOSINDY.

B. Symbolic Regression

Symbolic regression (SR) searches the space of all mathematical expressions representable by a given set of operators and variables, simultaneously inferring functional form and parameters. The foundations of modern SR trace to genetic programming, pioneered by Koza [20], which represents mathematical expressions as trees and applies evolutionary operators to iteratively improve a population of candidate expressions. The landmark Eureka platform of Schmidt and Lipson [21] established SR as a practical scientific tool, applying Pareto optimization to jointly minimize prediction error and expression complexity.

Among current SR tools, PYSR [22] has established itself as the leading open-source library for practical symbolic regression in the sciences. PYSR employs a multi-population evolutionary algorithm with an evolve-simplify-optimize loop: populations of expression trees evolve through mutation and crossover, each surviving expression is algebraically simplified via SymPy, and its numerical constants are refined by nonlinear optimization. An adaptive parsimony penalty discourages premature specialization, and a Julia backend (SymbolicRegression.jl) compiles user-defined operators into SIMD kernels at runtime. A recent systematic benchmark by Brum *et al.* [23] evaluated different SR methods on nine canonical dynamical systems including the Lorenz attractor, Lotka-Volterra equations, and a suite of epidemiological compartmental models under noisy conditions. PYSR was the top-performing method overall, recovering the correct structural form of all nine systems and demonstrating both accuracy and statistical robustness that no other evaluated method matched.

Despite this success, SR has inherent limitations when applied to multi-dimensional dynamical systems. Because SR methods optimize each state variable’s equation independently, they cannot enforce shared structure across coupled variables or exploit sparsity [8].

The NP-hardness of the general SR problem means that practical algorithms are heuristic and do not guarantee convergence to the globally optimal expression. Recovered expressions are often algebraically redundant or numerically ill-conditioned when integrated as ODEs, and tend to be of higher complexity than necessary [23, 26]. These limitations motivate the use of SR as a library *generation* tool rather than a standalone solver.

C. Hybrid and Automated Equation Discovery

Several prior works have sought to combine the strengths of symbolic and sparse regression, or to automate the library construction process. Fasel *et al.* [19] note that SR algorithms are inherently imbued with ensembling ideas, SR populations randomly combine library terms, and the best expressions at each complexity are retained across iterations, suggesting SR and sparse regression as complementary rather than competing approaches. However, no prior work had operationalized this complementarity into a formal hybrid discovery pipeline.

HAVOK (Hankel Alternative View Of Koopman) [27] and its successors combine delay embedding with sparse regression to discover linear representations of chaotic systems in lifted coordinates, effectively automating a restricted form of basis generation. Autoencoder-SINDY [15] jointly learns nonlinear coordinate transformations and sparse governing equations, automating basis discovery for systems with unknown intrinsic coordinates. Neural ODE-SINDY hybrids [28] use neural networks to parameterize unknown dynamics while SINDY identifies the interpretable sparse structure, an approach effective when partial domain knowledge is available. In the biological modeling context reviewed by Métayer *et al.* [8], hybrid and modular frameworks combining mechanistic grounding with data-driven library construction are identified as the primary direction for next-generation digital twin discovery.

A critical distinction between these prior works and AUTOSINDY is the treatment of the library as a fully learned, data-driven object with no domain-knowledge assumptions. Existing hybrid methods either require labeled intrinsic coordinates, known partial structure, or combine SR and sparse regression only conceptually without a formal curation pipeline. AUTOSINDY is the first framework to use symbolic regression purely as an unsupervised basis mining tool, to systematically decompose and filter its output through collinearity

analysis, and to hand the resulting library to SINDY for sparse coefficient recovery, all without any prior knowledge of the system’s mathematical form.

D. Deep Learning and Neural Approaches

Neural network-based approaches have also been applied to equation discovery and dynamical system identification. Physics-Informed Neural Networks (PINNs) [29] embed known PDEs into the loss function of a neural network, enabling data-efficient regression for parameterized systems with known governing structure. Neural ODEs [30] parameterize continuous-time dynamics as neural networks, enabling flexible modeling of black-box dynamical systems but at the cost of interpretability. Transformer-based SR models such as ODEFormer [31] uses a transformer pretrained on millions of synthetic trajectories to directly predict the symbolic form of a governing equation from data. It achieves strong results on low-dimensional benchmark systems but requires enormous pretraining and does not generalize reliably outside its training distribution. In contrast, AUTOSINDY requires no pretraining, produces human-readable closed-form equations, and operates from scratch on any system for which time-series data can be collected.

III. THE AUTOSINDY FRAMEWORK

AUTOSINDY is a three-stage, fully automated pipeline that converts raw, noisy time-series observations into a sparse, interpretable set of governing differential equations, without any prior specification of the system’s mathematical form. Figure 1 sketches the high-level concept: noisy observations feed a hybrid system in which a genetic algorithm (PySR) and a sparse regressor (SINDy) operate in sequence rather than in competition. Figure 2 gives a visual overview of the pipeline. In Stage 1 (DISCOVER), symbolic regression is applied to small, randomly sampled data windows to mine a diverse pool of candidate functional forms. In Stage 2 (CURATE), that raw pool is systematically decomposed, expanded, and filtered by a collinearity-aware pruning procedure that produces a compact, well-conditioned library. In Stage 3 (IDENTIFY), the curated library is handed to SINDY equipped with a bootstrap ensemble optimizer, which identifies the final sparse governing equations. Each stage is described in full below.

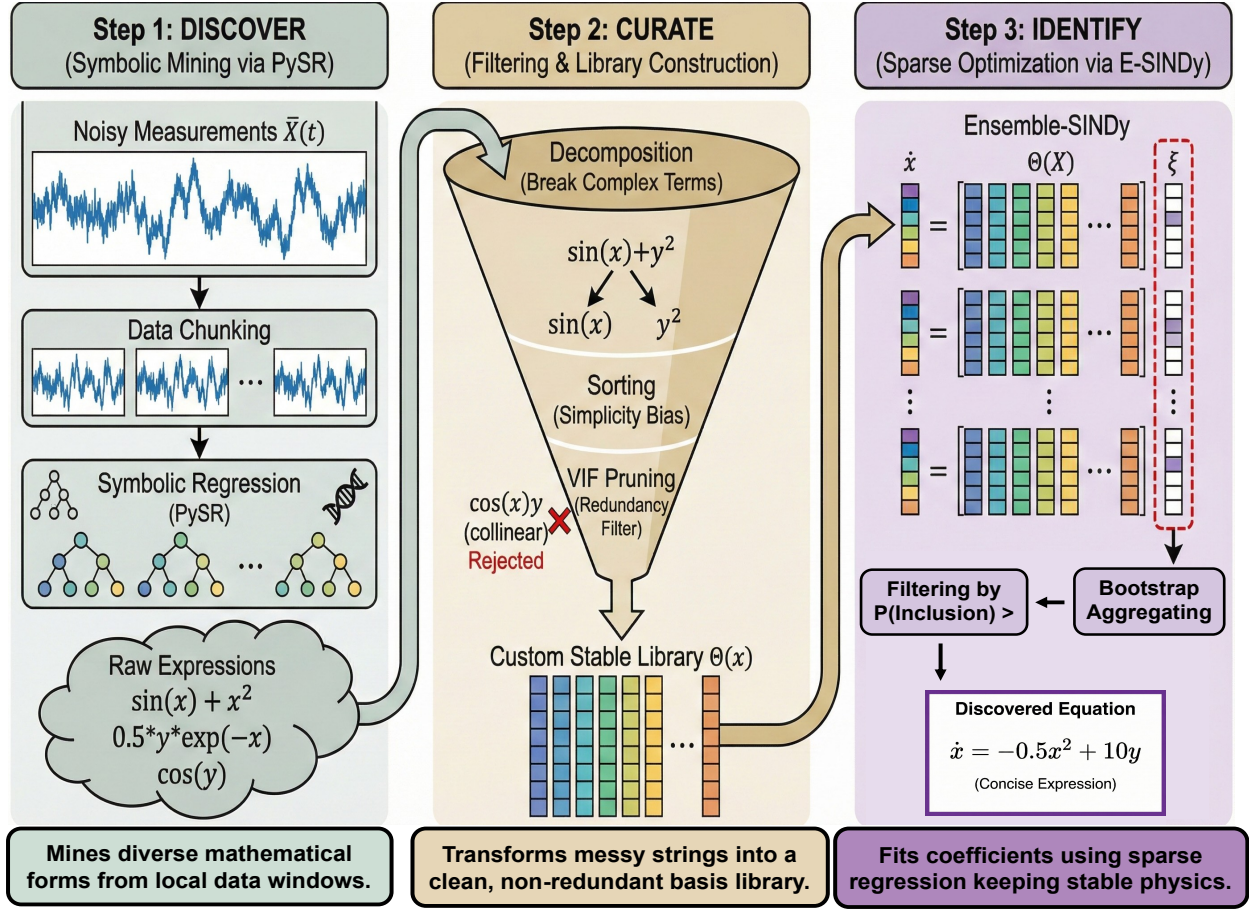


FIG. 2. The AutoSINDy hybrid architecture for robust automated discovery of governing equations. **Step 1 Discover:** PySR is applied independently to multiple short, randomly sampled data chunks, producing a pool of raw symbolic expressions (e.g., $\sin(x) + x^2$, $0.5y \exp(-x)$, $\cos(y)$). **Step 2 Curate:** Each expression is symbolically decomposed into atomic sub-terms ($\sin(x) + y^2 \rightarrow \sin(x), y^2$), the atoms are sorted by complexity to enforce a simplicity bias, and collinear terms (e.g., $\cos(x)y$, which is nearly linearly dependent on already-kept terms) are rejected by a VIF/correlation redundancy filter. The result is a compact, stable custom library $\Theta(x)$. **Step 3 Identify:** An Ensemble-SINDy optimizer fits sparse coefficients ξ across B bootstrap replicates; a hard-cutoff inclusion filter then retains only terms whose inclusion probability exceeds $\kappa = 0.80$, yielding a concise governing equation.

A. Problem Formulation

We seek to identify the governing ordinary differential equations of an n -dimensional dynamical system

$$\dot{\mathbf{x}}(t) = \mathbf{f}(\mathbf{x}(t)), \quad \mathbf{x}(0) = \mathbf{x}_0, \quad (1)$$

where $\mathbf{x}(t) \in \mathbb{R}^n$ is the state vector and $\mathbf{f} : \mathbb{R}^n \rightarrow \mathbb{R}^n$ is an unknown, potentially nonlinear vector field. We observe m snapshots

$$\mathbf{X} = [\mathbf{x}(t_1), \dots, \mathbf{x}(t_m)]^\top \in \mathbb{R}^{m \times n} \quad (2)$$

corrupted by additive Gaussian noise of relative amplitude σ (measured as a fraction of the per-dimension standard deviation of the clean trajectory). Time derivatives $\dot{\mathbf{X}}$ are estimated using PySINDy’s `SmoothedFiniteDifference` operator [11, 12], which applies a Savitzky-Golay smoothing filter before finite differencing to suppress noise amplification in the derivative estimate.

The objective is to recover \mathbf{f} as a sparse, closed-form symbolic expression. Following the SINDY formulation [9], this amounts to identifying a sparse coefficient matrix $\Xi \in \mathbb{R}^{p \times n}$ such that

$$\dot{\mathbf{X}} \approx \Theta(\mathbf{X}) \Xi, \quad (3)$$

where $\Theta(\mathbf{X}) \in \mathbb{R}^{m \times p}$ is a library matrix whose p columns are candidate functions evaluated over all observed states. Rather than specifying Θ from prior domain knowledge, AUTOSINDY constructs it automatically from data through the three stages described below.

B. Stage 1: Symbolic Mining via PYSR (DISCOVER)

The first stage uses PYSR [22], a state-of-the-art multi-population evolutionary symbolic regression tool, to extract a diverse pool of candidate functional forms directly from trajectory data. Two design choices, chunked stochastic sampling and full Pareto harvesting, ensure that the discovery phase is both computationally tractable and semantically comprehensive.

1. Chunked Stochastic Sampling

Rather than applying symbolic regression to the full training trajectory, AUTOSINDY operates on K short, randomly sampled windows of the data. Each chunk is constructed by drawing, without replacement, an index set \mathcal{I}_k of size $c = \lfloor m_{\text{train}}/d \rfloor$ from the training samples:

$$\mathcal{D}_k = \{(\mathbf{x}_i, \dot{\mathbf{x}}_i) : i \in \mathcal{I}_k\}, \quad k = 1, \dots, K, \quad (4)$$

where d is the chunk-size divisor and K is the number of discovery rounds. This strategy serves three purposes simultaneously: (i) each compact window exposes a concentrated local slice of state space, making the evolutionary search substantially more tractable than fitting the full trajectory; (ii) different windows sample different dynamical regimes, generating a semantically diverse candidate pool; and (iii) the random selection prevents systematic over-representation of any single region of the attractor, improving the breadth of functional forms discovered.

2. Symbolic Regression and Pareto Harvesting

For each chunk \mathcal{D}_k and each target derivative \dot{x}_j , AUTOSINDY invokes PYSR with a fixed operator vocabulary comprising the binary operators and the unary operators. Nested trigonometric compositions (e.g. $\sin(\sin(\cdot))$) are explicitly forbidden via nested constraints, preventing the evolutionary search from exploiting degenerate identities. These constraints are applied to ensure the search space remains consistent with traditional methods, thereby facilitating a more practical comparison.

Crucially, AUTOSINDY harvests *every* expression that appears on the returned Pareto-optimal front, not only the single highest-scoring model. Sub-optimal expressions at lower complexity levels frequently contain structurally correct atomic sub-terms that are globally valid for the governing equation, even when the full expression is a poor fit to a particular local chunk. The union of all Pareto expressions across all chunks and all target variables defines the raw symbolic pool:

$$\mathcal{E}_{\text{raw}} = \bigcup_{j=1}^n \bigcup_{k=1}^K \bigcup_c e_{j,k,c}, \quad (5)$$

where $e_{j,k,c}$ denotes the Pareto expression of complexity c obtained for target j on chunk k .

All expressions are stored as SymPy [32] symbolic objects for symbolic manipulation in the subsequent curation stage.

C. Stage 2: Multi-Stage Library Curation (CURATE)

The raw pool \mathcal{E}_{raw} typically contains hundreds of compound, overlapping symbolic expressions. Using them directly as library columns would produce a severely rank-deficient library matrix and destabilize the sparse regression. Stage 2 reduces this pool to a compact, well-conditioned set of basis functions through three sequential operations: symbolic decomposition, algebraic expansion, and collinearity pruning. The full procedure is given in Algorithm 1.

1. Step 2a: Symbolic Decomposition

Each expression $e \in \mathcal{E}_{\text{raw}}$ is parsed via SymPy and decomposed into its additive sub-terms (atoms):

$$\mathcal{A}_e = \{a : a \text{ is an additive atom of } e\}. \quad (6)$$

For example, the expression $3x_0^2 + 2\sin(x_1)$ yields atoms $\{x_0^2, \sin(x_1)\}$. All numeric constant prefactors are stripped, since SINDY learns all coefficients independently during the regression step. The full atomic set is formed by $\mathcal{A} = \bigcup_{e \in \mathcal{E}_{\text{raw}}} \mathcal{A}_e$, de-duplicated by symbolic equivalence. This step focuses the library on unique functional forms rather than rescaled variants of the same expression.

2. Step 2b: Algebraic Expansion

Compound atomic terms may contain grouped polynomial sub-expressions whose monomials are useful basis functions in their own right. AUTOSINDY supports three configurable expansion strategies applied to each atom via SymPy’s algebraic and trigonometric expansion routines:

- **Severe:** Full polynomial and trigonometric expansion. $(x_0+x_1)^2$ becomes $\{x_0^2, 2x_0x_1, x_1^2\}$ and $\sin(x_0 + x_1)$ is expanded via the angle-sum identity. This maximizes coverage of monomial basis functions at the cost of a larger intermediate pool.

- **Gentle:** Only constant-factor expansion; grouped polynomial expressions are preserved intact. $(x_0 + x_1)^2$ remains as a single atom. This is the default strategy and performs best on systems where the true basis functions are grouped.
- **Hybrid:** Both the gentle and severe forms of each atom are added to the pool, providing maximum coverage at the cost of a temporarily larger candidate set before pruning.

After expansion, all atoms are collected into the augmented candidate set $\mathcal{A} = \{a_1, \dots, a_P\}$ and sorted in *ascending order of SymPy operator count*. This complexity ordering enforces a *simplicity bias*: simpler expressions are always considered before more complex ones in the subsequent pruning step, ensuring that when two expressions carry equivalent empirical information, the algebraically simpler one is preferred.

3. Step 2c: Collinearity Pruning with Simplicity Bias

Multicollinearity among library terms is the primary driver of coefficient instability in sparse regression: near-linearly dependent columns inflate coefficient variance and frustrate the sparsity optimizer. AUTOSINDY removes such redundancy through a greedy forward-selection procedure that processes the complexity-sorted candidates in order.

Let $\mathcal{L} = \emptyset$ be the accepted library, initially empty. For each candidate atom $a_i \in \mathcal{A}$ (in complexity order):

1. Evaluate $\mathbf{v}_i = a_i(\mathbf{X}_{\text{train}}) \in \mathbb{R}^{m_{\text{train}}}$.
2. Discard a_i if $\text{std}(\mathbf{v}_i) < \varepsilon$ (constant or numerically degenerate over the training domain).
3. Otherwise, compute the pairwise Pearson correlation between \mathbf{v}_i and every already-accepted feature $\mathbf{v}_j = a_j(\mathbf{X}_{\text{train}})$, $a_j \in \mathcal{L}$. Accept a_i if and only if

$$|\text{corr}(\mathbf{v}_i, \mathbf{v}_j)| < \rho_{\max} \quad \forall a_j \in \mathcal{L}, \quad (7)$$

where ρ_{\max} is the collinearity threshold.

4. If accepted, append a_i to \mathcal{L} .

The complexity-ordered traversal guarantees the simplicity bias: a complex atom a_i is retained *only* if it provides information that no simpler already-accepted term can replicate. This directly implements Occam’s razor at the library level, independently of the downstream sparse optimizer.

An alternative pruning criterion based on the Variance Inflation Factor (VIF) is also supported. In this mode, a temporary ordinary least squares regression is fitted with a_i as the response and all columns of \mathcal{L} as predictors; the resulting R_i^2 yields

$$\text{VIF}_i = \frac{1}{1 - R_i^2}. \tag{8}$$

The atom a_i is accepted if and only if $\text{VIF}_i < \tau_{\text{VIF}}$. The VIF criterion detects *multicollinearity with respect to the entire accepted set* rather than any single pair, making it more sensitive to jointly redundant groups of terms. In our experiments, pairwise correlation pruning was used as the primary method due to its lower computational overhead and competitive results; VIF pruning is retained as a configurable option.

The final curated library $\mathcal{L} = \{\ell_1, \dots, \ell_q\}$, with $q \leq P$, is used to construct the library matrix $\Theta(\mathbf{X})$.

Algorithm 1: Library Curation with Simplicity Bias

Input: Raw pool \mathcal{E}_{raw} , training data $\mathbf{X}_{\text{train}}$, threshold ρ_{max} , expansion strategy

$s \in \{\text{gentle}, \text{severe}, \text{hybrid}\}$

Output: Curated library \mathcal{L}

$\mathcal{A} \leftarrow \emptyset;$

for $e \in \mathcal{E}_{\text{raw}}$ **do**

 Parse e with SymPy; decompose into additive atoms; strip numeric constants;

 Apply expansion strategy s to each atom;

$\mathcal{A} \leftarrow \mathcal{A} \cup \{\text{expanded atoms}\};$

end

Sort \mathcal{A} by SymPy operator count (ascending);

$\mathcal{L} \leftarrow \emptyset;$

for $a_i \in \mathcal{A}$ (*in sorted order*) **do**

$\mathbf{v}_i \leftarrow a_i(\mathbf{X}_{\text{train}});$

if $\text{std}(\mathbf{v}_i) < \varepsilon$ **then skip** (constant or degenerate);

if $\max_{a_j \in \mathcal{L}} |\text{corr}(\mathbf{v}_i, \mathbf{v}_j)| < \rho_{\text{max}}$ **then**

$\mathcal{L} \leftarrow \mathcal{L} \cup \{a_i\};$

end

end

return \mathcal{L}

D. Stage 3: Sparse Identification via Ensemble SINDY (IDENTIFY)

1. Library Matrix Construction

The curated library $\mathcal{L} = \{\ell_1, \dots, \ell_q\}$ is augmented with a constant bias term to form a library of $p = q + 1$ functions. The library matrix evaluated over the training data is

$$\Theta(\mathbf{X}_{\text{train}}) = [\mathbf{1}, \ell_1(\mathbf{X}_{\text{train}}), \dots, \ell_q(\mathbf{X}_{\text{train}})] \in \mathbb{R}^{m_{\text{train}} \times (q+1)}, \quad (9)$$

where each column is the function evaluated point-wise over all training observations.

2. Sparse Regression via STLSQ or SR3

The sparse coefficient matrix $\hat{\Xi}$ is obtained by solving the ℓ_0 -penalized regression problem

$$\hat{\Xi} = \arg \min_{\Xi} \|\hat{\mathbf{X}}_{\text{train}} - \Theta(\mathbf{X}_{\text{train}})\Xi\|_F^2 + \lambda \|\Xi\|_0, \quad (10)$$

where $\|\cdot\|_F$ is the Frobenius norm.

Two sparse optimizers are supported. **Sequential Thresholded Least Squares (STLSQ)** [9] is the default: it alternates between a ridge-regularized least-squares fit and a hard coefficient threshold at level λ until the active set converges. The threshold λ acts as the principal sparsity-promoting hyperparameter. Alternatively, **Sparse Relaxed Regularized Regression (SR3)** [16] reformulates the problem with a convex relaxation that introduces an auxiliary variable, decoupling the fitting and thresholding sub-problems. SR3 is particularly effective when library columns have moderate correlations that survive the curation step; it is accessible as a configurable option with relaxation parameter ν and a fixed maximum iterations.

3. Bootstrap Ensemble with Inclusion-Probability Masking

To suppress library terms that are selected spuriously due to noise, AUTOSINDY wraps the chosen optimizer inside a bootstrap ensemble following the E-SINDY paradigm [19]. A total of B bootstrap replicates are drawn from the training set, and an independent sparse model is fitted on each replicate. The empirical inclusion probability of the (i, j) -th coefficient (library term i , state variable j) is

$$\hat{p}_{ij} = \frac{1}{B} \sum_{b=1}^B \mathbf{1}[|\Xi_{ij}^{(b)}| > 0]. \quad (11)$$

A hard-cutoff mask then enforces a binary active/inactive decision:

$$\hat{\Xi}_{ij} = \begin{cases} \bar{\Xi}_{ij} & \text{if } \hat{p}_{ij} \geq \kappa, \\ 0 & \text{otherwise,} \end{cases} \quad (12)$$

where $\bar{\Xi}_{ij}$ is the ensemble mean coefficient computed over replicates in which the term was active, and κ is the inclusion cutoff. Terms appearing in fewer than $\kappa\%$ of bootstrap fits are deemed noise artifacts and set to zero, yielding maximally sparse and physically

interpretable final equations. The combination of a curated, low-redundancy library and ensemble-based term filtering provides two complementary layers of noise rejection: the curation stage eliminates structurally redundant candidates before fitting begins, while the inclusion filter eliminates statistically unreliable coefficients after fitting.

4. *Unified vs. Per-Variable Library Strategies*

AUTOSINDY supports two strategies for library construction and fitting, offering a trade-off between cross-equation consistency and per-equation specificity.

a. Separate libraries (default). For each target derivative \dot{x}_j , Stage 1 runs PySR independently and Stage 2 curates a variable-specific library \mathcal{L}_j . A separate SINDY model is then fitted for each j , solving $\dot{x}_j \approx \Theta_j(\mathbf{X}) \boldsymbol{\xi}_j$. This strategy allows each equation to contain only the functional forms that are locally relevant, and typically produces the most parsimonious individual equations.

b. Unified library. Alternatively, Stage 1 harvests expressions for all target variables simultaneously; Stage 2 pools and curates them into a single shared library \mathcal{L} ; and a single SINDY model is fitted across all state variables jointly via Eq. (3). The unified strategy is better suited to tightly coupled systems where the same functional forms appear in multiple equations, as it enforces structural consistency at the cost of including terms that may be irrelevant for some equations.

In our experiments, the separate-library strategy is used as the default because it produces consistently lower complexity and more accurate identification across the benchmark suite.

E. Complete Pipeline Summary

The full AUTOSINDY procedure is summarized in Algorithm 2.

Algorithm 2: AUTOSINDY: Automated Sparse System Identification

Input: Noisy observations \mathbf{X} , estimated derivatives $\dot{\mathbf{X}}$, hyperparameters

$$K, d, \rho_{\max}, \lambda, B, \kappa$$

Output: Sparse symbolic model $\hat{\Xi}$ and governing equations $\hat{\mathbf{f}}$

// Stage 1: Symbolic Discovery

$\mathcal{E}_{\text{raw}} \leftarrow \emptyset;$

for $k = 1, \dots, K$ **do**

 Sample random chunk \mathcal{D}_k of size $\lfloor m_{\text{train}}/d \rfloor;$

for $j = 1, \dots, n$ **do**

 Run PYSR on $(\mathcal{D}_k, \dot{x}_j);$ harvest full Pareto front $\mathcal{P}_{jk};$

$\mathcal{E}_{\text{raw}} \leftarrow \mathcal{E}_{\text{raw}} \cup \mathcal{P}_{jk};$

end

end

// Stage 2: Library Curation (Algorithm 1)

$\mathcal{L} \leftarrow \text{CURATE}(\mathcal{E}_{\text{raw}}, \mathbf{X}_{\text{train}}, \rho_{\max});$

Build library matrix $\Theta(\mathbf{X}_{\text{train}})$ from $\mathcal{L} \cup \{1\};$

// Stage 3: Ensemble Sparse Identification

for $b = 1, \dots, B$ **do**

 Draw bootstrap replicate; fit sparse optimizer $\rightarrow \Xi^{(b)};$

end

Compute \hat{p}_{ij} via Eq. (11);

Apply hard-cutoff mask via Eq. (12) to obtain $\hat{\Xi};$

return $\hat{\Xi};$

$$\hat{\mathbf{f}}(\mathbf{x}) = \Theta(\mathbf{x})\hat{\Xi}$$

IV. EXPERIMENTAL SETUP

Evaluating a symbolic discovery framework requires more than measuring predictive accuracy on training data: a method that memorizes the training trajectory adds no scientific value, and a method that produces interpretable equations which immediately diverge under integration is not physically meaningful. Our experimental design therefore makes two deliberate choices. First, all generalization metrics are computed on a *completely unseen*

validation trajectory generated from a different initial condition with zero noise, ensuring that reported scores reflect the ability to capture true governing physics rather than noise-specific patterns. Second, we evaluate both *derivative prediction* (a local, instantaneous test of structural correctness) and *long-horizon simulation* (a global, integral test of dynamical stability), since the two can diverge dramatically: an equation may fit local derivatives well yet diverge catastrophically under forward integration. The full experimental protocol is described below.

A. Benchmark Dynamical Systems

We evaluate AUTOSINDY on six canonical nonlinear dynamical systems spanning a wide range of structural complexity and dynamic character (Table I). The true canonical complexity, measured as the total symbolic operator count of the fully expanded governing equations, ranges from 3 for the simple harmonic oscillator to 15 for the Complex Lorenz system, which couples chaotic dynamics with a transcendental cross-term $\gamma x_1 \sin(x_0 + x_2)$.

TABLE I. Benchmark dynamical systems, governing equations, key dynamical characteristics, and ground-truth canonical complexity (SymPy operator count of the expanded form).

System	n	Governing Equations	Characteristics	True Complexity
Harmonic Oscillator	2	$\dot{x}_0 = x_1$ $\dot{x}_1 = -k_1 x_0 - k_2 x_1$	Linear, periodic	3
Damped Pendulum	2	$\dot{x}_0 = x_1$ $\dot{x}_1 = -bx_1 - c \sin(x_0)$	Trigonometric, dissipative	4
Modulated Oscillator	2	$\dot{x}_0 = x_1$ $\dot{x}_1 = -bx_1 \cos(x_0) - kx_0$	Trigonometric damping	5
Van der Pol	2	$\dot{x}_0 = x_1$ $\dot{x}_1 = \mu(1 - x_0^2)x_1 - x_0$	Nonlinear limit cycle	6
Duffing Oscillator	2	$\dot{x}_0 = x_1$ $\dot{x}_1 = -\delta x_1 - \alpha x_0 - \beta x_0^3$	Bistable, polynomial	6
Complex Lorenz	3	$\dot{x}_0 = \sigma(x_1 - x_0)$ $\dot{x}_1 = x_0(\rho - x_2) - x_1$ $\dot{x}_2 = x_0 x_1 - \beta x_2 + \gamma x_1 \sin(x_0 + x_2)$	Chaotic, trigonometric	15

B. Data Generation and Noise Protocol

Figure 3 illustrates the complete data generation and evaluation pipeline. For each system, a training trajectory of 5000 uniformly spaced snapshots is simulated via SciPy’s `solve_ivp`. Additive Gaussian noise is injected relative to each state variable’s standard deviation:

$$\mathbf{X}_{\text{noisy}} = \mathbf{X}_{\text{clean}} + \boldsymbol{\varepsilon}, \quad \varepsilon_{ij} \sim \mathcal{N}(0, \sigma^2 \text{Var}(X_{.j})), \quad (13)$$

at six levels $\sigma \in \{0, 0.01, 0.02, 0.03, 0.04, 0.05\}$ representing the noise-to-signal ratio. Each level is repeated across five independent random seeds ($s \in \{32, \dots, 36\}$), giving 6 systems \times 6 noise levels \times 5 seeds = 180 trials per method, and 540 total runs. Furthermore, A crash-recovery mechanism tracks in-progress runs and automatically applies fallback seeds to any trial that was interrupted, ensuring full sweep completion without duplicating successful runs.

The qualitative impact of noise on raw signal fidelity is illustrated in Appendix A, which shows the state trajectories, numerically estimated derivatives, and phase portraits for the damped pendulum at noise levels $\sigma \in \{0.00, 0.01, 0.05\}$. At $\sigma = 0.05$, the raw derivative signal is heavily corrupted, motivating the need for robust library selection and regularization as implemented in AutoSINDy.

The *training trajectory* is noisy and split 80/20 using a *middle split*: the central 80% of the time series forms the training set, while the flanking 10% segments form the hold-out test, demanding accuracy in both interpolation and boundary extrapolation.

A second, *fully independent validation trajectory* is generated from the same system with distinct initial conditions and *zero* measurement noise ($\sigma = 0$). This clean trajectory is never exposed to the discovery or fitting stages; it is used exclusively to assess whether the discovered model captures the true underlying physics rather than characteristics of the training noise. Simulation performance is assessed by numerically integrating the discovered model forward in time from the validation trajectory’s initial condition and comparing against the corresponding clean ground-truth trajectory.

C. Baseline Methods

AUTOSINDY is benchmarked against two established methods:

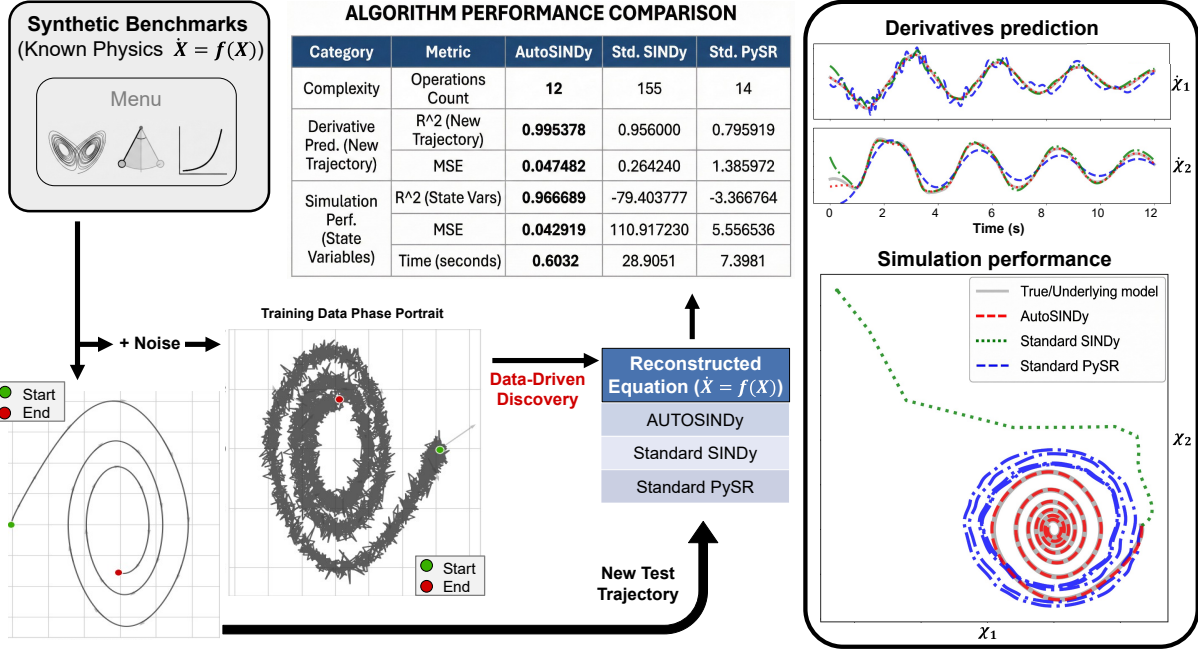


FIG. 3. Experimental protocol and an illustrative example. A trajectory is generated from a system with known physics and then corrupted by Gaussian noise to produce the training set (centre left). Three methods (AUTOSINDY, Standard SINDY, Standard PySR) independently attempt to recover the governing equations from this noisy data. Discovered models are validated on a *clean* trajectory from a previously unseen initial condition: once for derivative prediction accuracy and once for long-horizon simulation. The right panel shows a representative single-trial comparison on the harmonic oscillator, where AUTOSINDY achieves the best accuracy at a fraction of the complexity of Standard SINDY.

1. **Standard SINDy with enriched library**: Uses a fixed candidate library combining polynomial terms up to degree 3 and Fourier basis functions with one frequency: $\mathcal{F}_{\text{std}} = \text{PolyLib}(d=3) \oplus [\text{PolyLib}(d=3) \times \text{FourierLib}(f=1)]$. This large, generic library is the standard choice when the system structure is unknown. The identical ensemble STLSQ optimizer ($B = 20$, $\lambda = 0.21$) is used to ensure that performance differences reflect library construction rather than the optimizer.
2. **Standard PySR**: Direct symbolic regression applied to the full training set, using the same operator vocabulary and hyperparameters as the AUTOSINDY discovery stage, but without the curation or sparse-identification stages. The best equation on the Pareto front is selected independently for each state derivative.

D. Evaluation Metrics

Model performance is assessed with five complementary criteria that together probe *local structural correctness* (derivative prediction), *global dynamical validity* (long-horizon simulation), *equation recovery* (a strict threshold-based proxy for exact identification), *symbolic parsimony* (operator-level complexity), and *computational efficiency* (wall-clock timing). Using all five is essential because the criteria can diverge dramatically: a model may achieve high derivative R^2 yet diverge catastrophically under integration, or may produce a compact equation that is nonetheless structurally incorrect. No single score is sufficient on its own.

1. Derivative Prediction Accuracy

The coefficient of determination R^2 and mean squared error (MSE) between the true time derivatives and the model’s instantaneous predictions are computed on both the held-out test segment of the training trajectory and the independent clean validation trajectory:

$$R^2 = 1 - \frac{\|\dot{\mathbf{X}} - \hat{\dot{\mathbf{X}}}\|_F^2}{\|\dot{\mathbf{X}} - \bar{\dot{\mathbf{X}}}\|_F^2}, \quad \text{MSE} = \frac{1}{Nn} \|\dot{\mathbf{X}} - \hat{\dot{\mathbf{X}}}\|_F^2. \quad (14)$$

Scores on the validation trajectory are the primary indicator of structural correctness: a model that has captured the wrong functional form cannot sustain $R^2 \approx 1$ on a previously unseen, noise-free trajectory generated from a different initial condition, so this score simultaneously tests both generalization and equation fidelity. Scores on the test segment of the training trajectory serve as a secondary check for overfitting.

2. Equation Recovery Rate

For each system and noise level, we report the fraction of trials (across seeds) in which the discovered model achieves $R^2 > 0.99$ on the clean validation trajectory. This strict binary threshold acts as a conservative proxy for *correct structural identification*. The threshold is motivated empirically: a model with an incorrect functional form (for example, a polynomial approximation of a $\sin(\cdot)$ term) reliably achieves $R^2 < 0.98$ on the clean validation trajectory, while a model that has recovered the correct governing terms consistently exceeds 0.99. The recovery rate therefore measures the fraction of trials in which the discovery pipeline succeeds in identifying the true physics, rather than merely fitting the training data.

3. Long-Horizon Simulation Stability

The discovered governing equations are numerically integrated forward from the validation trajectory’s initial condition using SciPy’s stiff Radau ODE solver. Simulated trajectories are compared against the corresponding noise-free ground-truth trajectory, with R^2 and MSE computed over the state variables. Integration is terminated early if any state variable exceeds $100\times$ the ground-truth amplitude, which serves as a divergence detection criterion. Trials in which integration crashes (NaN/Inf values or early divergence termination) are recorded as hard failures: they are excluded from the mean R^2 and MSE summaries but counted explicitly in the reported failure rate, ensuring that they do not silently inflate mean performance. Simulation R^2 therefore captures whether the discovered equation is not only locally accurate in its derivative predictions but also globally stable and physically coherent when used as a predictive model.

4. Symbolic Parsimony

We measure equation complexity as the total operator count of the fully algebraically expanded governing equations, computed via SymPy’s `count_ops` after applying `sympy.expand()`. Formally, for a discovered equation \hat{f} with canonical (expanded) form $\tilde{f} = \text{expand}(\hat{f})$, we define

$$C(\hat{f}) = \text{count_ops}(\tilde{f}), \tag{15}$$

where `count_ops` tallies every arithmetic and transcendental operation in the expression tree (additions, multiplications, exponentiations, sin, cos, etc.).

a. Why not the standard SINDy term count? The conventional complexity metric in sparse identification is the ℓ_0 norm of the coefficient vector which is the number of nonzero library terms. This measure assigns equal complexity to x_1 and $x_1^2x_2x_3$, treating a simple linear variable and a fourth-degree monomial as indistinguishable in cost. Such a metric cannot differentiate a genuinely parsimonious physical model from a bloated one that happens to use few, but individually complex, terms. Operator count, by contrast, grows proportionally with the actual arithmetic operations required to evaluate the expression, providing a complexity measure that is directly consistent with the computational, analytic, and interpretability cost of the discovered equation.

b. Why expand before counting? PYSR naturally returns factored expressions, e.g. $\mu(1 - x_0^2)x_1$ for the Van der Pol nonlinearity, while SINDY always returns expanded polynomial forms, e.g. $\mu x_1 - \mu x_0^2 x_1$. Both representations encode exactly the same physics, yet their raw operator counts differ. Measuring complexity on the as-written form would therefore systematically and unfairly favour PYSR over SINDY-based methods with no scientific justification. Applying `sympy.expand()` before counting places all methods on an identical canonical representation, and the resulting operator count can be directly compared against the known ground-truth complexity of the benchmark systems reported in Table I.

c. Sign normalization. An expression whose leading term is negative is negated before counting, using SymPy’s `could_extract_minus_sign`, since $-2x_0 - 3x_1$ and $2x_0 + 3x_1$ represent equally complex models under a sign flip of the coefficient. This prevents the canonical form from artificially inflating complexity for equations whose dominant term happens to be negative.

5. Computational Efficiency

We report wall-clock timing separately for two stages to allow independent interpretation:

1. Discovery time: the total elapsed time for Stage 1 (PYSR across all chunks and state variables), Stage 2 (curation), and Stage 3 (ensemble SINDY fitting). This is the time a practitioner must wait before a governing equation is available.
2. Simulation time: the time required to numerically integrate the discovered governing equations forward over the simulation horizon using the Radau solver. This reflects the practical cost of using the equation for downstream prediction or control, and is directly affected by equation complexity: bloated equations with many terms produce stiffer ODE systems that require finer time-stepping, leading to substantially longer integration times even when two equations nominally achieve similar R^2 scores.

These two timing quantities capture complementary aspects of computational cost and are not aggregated, since a fast discovery with a complex equation and a slow discovery with a parsimonious equation represent qualitatively different trade-offs.

E. Implementation Details

AUTOSINDY is implemented in Python using PYSINDY v1.7.5 [11, 12], PySR v1.5.8 [22], and SYMPY v1.14.0 [32] for symbolic manipulation. PySR is run in deterministic serial mode (`parallelism="serial", deterministic=True`) to ensure reproducibility. Source code and all experimental configurations are available at <https://github.com/mabasiri95/AutoSINDy>.

V. RESULTS

We organize the results around four core claims: (i) AUTOSINDY achieves superior derivative prediction accuracy across systems and noise levels; (ii) it dramatically outperforms baselines in long-horizon simulation stability; (iii) it discovers equations of near-ground-truth complexity while both baselines systematically over- or under-compress; and (iv) these gains are achieved at a modest computational overhead. Figure 3 provides an illustrative example that motivates the full quantitative analysis and answering the following questions: Does AUTOSINDY recover the correct governing structure? Do discovered models remain stable under long-horizon simulation? How parsimonious are the recovered equations? How does noise robustness compare across methods?

A. Overall Reliability: Derivative and Simulation Accuracy

Figure 4 provides the clearest macroscopic summary of relative performance. Trials are classified into four tiers based on new-trajectory R^2 : Excellent ($R^2 \geq 0.99$), Good ($0.90 \leq R^2 < 0.99$), Poor ($0 \leq R^2 < 0.90$), and Failed ($R^2 < 0$).

a. Derivative prediction. AUTOSINDY places **92.8%** of all trials in the Excellent tier for derivative prediction on the clean validation trajectory, compared to 58.9% for Standard SINDy and only 28.3% for Standard PySR. Standard SINDy, despite its large fixed library, places 17.2% of trials in the Failed tier which is a consequence of the ill-conditioning induced by the high-dimensional enriched library at elevated noise levels. Standard PySR is unable to achieve excellent accuracy in the majority of cases (61.1% of trials fall below $R^2 = 0.99$), reflecting its susceptibility to noise-driven over-complexity.

b. Simulation stability. The gap between methods widens dramatically when evaluating long-horizon simulation (Fig. 4, bottom bars per method). AUTOSINDY achieves

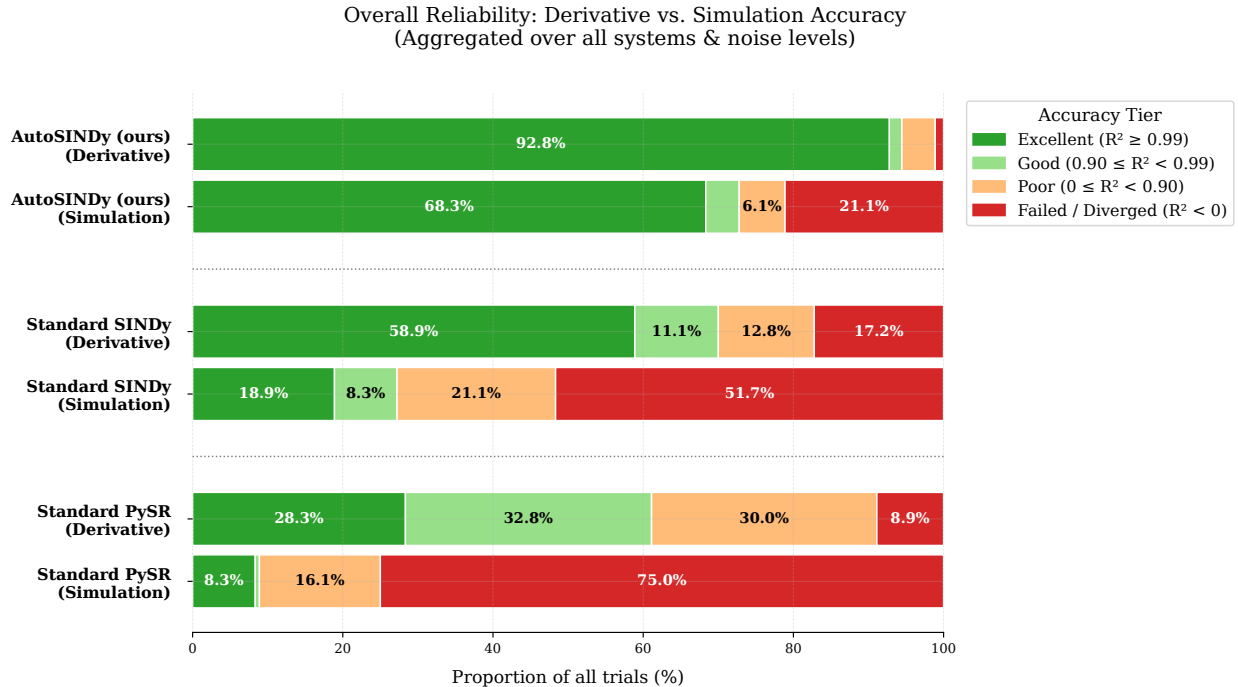


FIG. 4. Overall reliability of the three methods, aggregated over all six dynamical systems and all six noise levels ($N = 180$ trials per method). Horizontal bars show the proportion of trials in each accuracy tier for derivative prediction (top bar per method) and long-horizon simulation (bottom bar per method). AUTOSINDY achieves the highest proportion of excellent outcomes in both categories while maintaining the lowest failure rate.

Excellent simulation performance in **68.3%** of all trials, while Standard SINDy and Standard PySR achieve only 18.9% and 8.3% respectively. Most strikingly, Standard SINDy *fails* (diverges) in 51.7% of trials and Standard PySR in 75.0%, underscoring that good derivative prediction alone does not guarantee stable forward integration. AUTOSINDY fails in only 21.1% of trials, and, as detailed next, these failures are concentrated in the most challenging systems at the highest noise levels.

B. Noise Robustness

Figure 5 shows the distribution of derivative-prediction and simulation R^2 scores aggregated across all systems and plotted as a function of noise level σ . AUTOSINDY's derivative-prediction distribution remains tightly concentrated near $R^2 = 1$ for all noise levels, with only a small tail of outlier trials (primarily on the Duffing system at the high-

Noise Robustness Distributions Across All Systems
(Boxplot + Raw Trial Overlay)

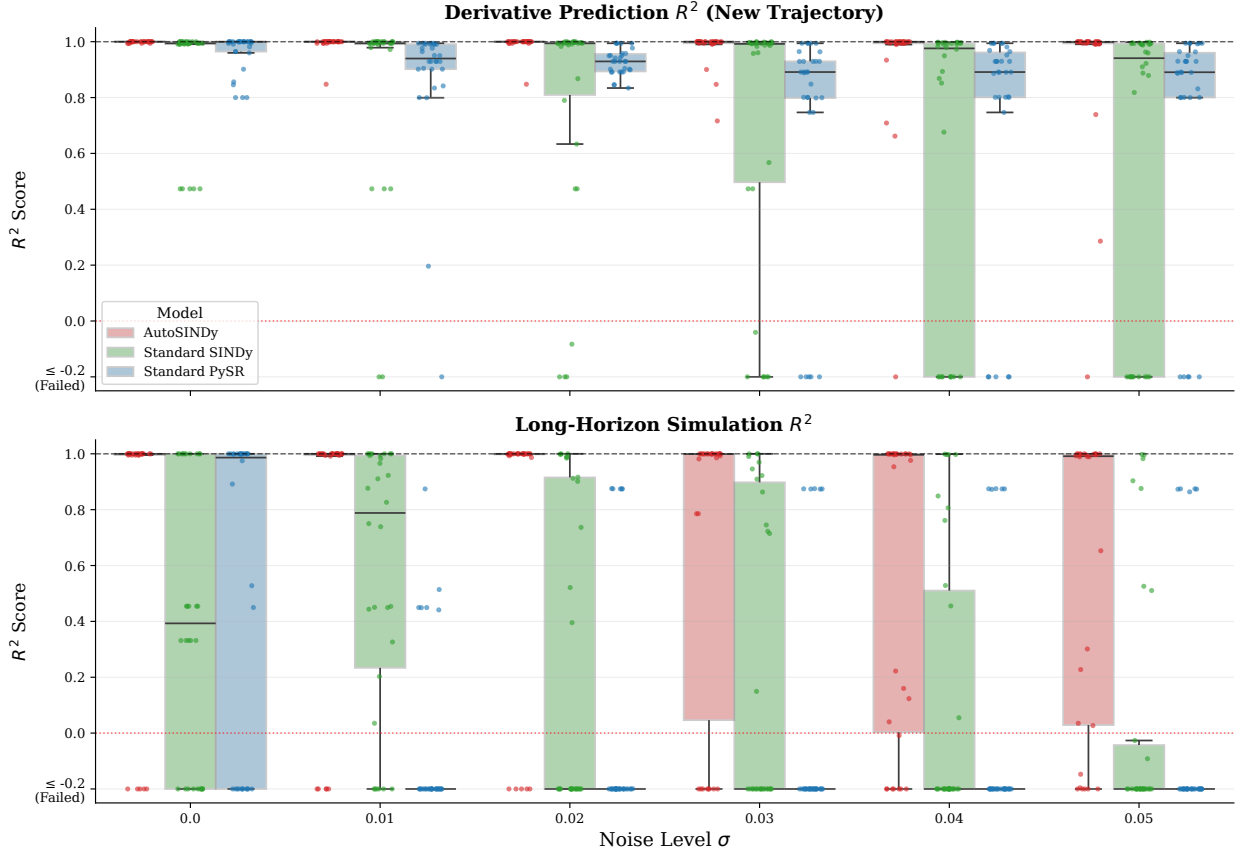


FIG. 5. Aggregate noise robustness distributions summarizing performance across all six systems. Boxplots are overlaid with raw trial data points. **Top:** Derivative prediction R^2 on the clean validation trajectory remains consistently near unity for AUTOSINDY (red) across all noise levels. **Bottom:** Long-horizon simulation R^2 shows AUTOSINDY maintaining high performance at elevated noise while Standard SINDY (green) and Standard PySR (blue) exhibit increasing divergence rates. Trials with $R^2 \leq -0.2$ (below the red dotted line) are explicitly grouped as “Failed”. AUTOSINDY maintains the tightest, highest distribution; both baselines exhibit widespread failures, increasingly so with noise.

est noise levels). In contrast, Standard SINDY exhibits a wide variance that grows with noise, and Standard PySR’s simulation performance degrades at $\sigma = 0.02$. Even at zero noise, the recovery rates reveal important structural differences. Standard SINDY’s 83% and PySR’s 67% confirm that their failure modes are not purely noise-driven, they stem from fundamental library and regularization limitations. As noise grows, AUTOSINDY degrades

most gracefully, maintaining 90% recovery at $\sigma = 0.05$ compared to 40% (SINDy) and 20% (PySR). Notably, the derivative R^2 distribution of AUTOSINDY in Figure 5 remains tightly concentrated near 1.0 at all noise levels, which is a qualitatively different behaviour from the wide, heavy-tailed distributions of both baselines.

The per-system performance dashboard (Fig. 6) reveals complementary system-specific patterns and the full noise-level breakdown for all six metrics per system. For the harmonic oscillator, all three methods achieve near-perfect derivative prediction during training. However, Standard SINDy experiences a striking validation failure. This counterintuitive result is explained by severe library bloat: the canonical complexity reaches approximately 70 compared to the ground-truth value of 3. The enriched polynomial-Fourier basis contains high-degree cross-terms and trigonometric functions that are individually predictive on the noisy training data but mutually contradictory when fit simultaneously. Under the ensemble optimizer, many of these spurious terms receive nonzero coefficients, producing an internally inconsistent model that fails on the clean validation trajectory. In contrast, AUTOSINDY recovers the true equations in every trial for this system.

This strong performance by AUTOSINDY extends to other systems, recovering the true equations in every trial for the modulated oscillator, whereas Standard SINDy again produces heavily over-complex equations (median ≈ 70) compared to the ground-truth complexity of 6. On the damped pendulum, which requires discovering the non-polynomial $\sin(x_0)$ term from noisy data, AUTOSINDY achieves 96.7% recovery compared to 46.7% for Standard SINDy and 33.3% for Standard PySR. Standard SINDy also suffers from library bloat here, reaching a high complexity versus the true value of 4, leading to frequent simulation instabilities.

For the Van der Pol oscillator, AUTOSINDY recovers a concise equation with a median complexity of approximately 12 and achieves perfect simulation stability, again recovering the true equations in every trial. Conversely, Standard SINDy’s complexity explodes to a median of 175 operators against a ground truth of 6, producing unstable simulations in 6 out of 30 trials (see Section VC). Furthermore, Standard PySR achieves 0% recovery on this system despite producing a median $R^2 = 0.8$, which consistently falls below the $R^2 > 0.99$ threshold. This confirms that pure symbolic regression, without sparsity promotion, consistently fails to isolate the $x_0^2 x_1$ term with sufficient coefficient precision.

The Duffing oscillator proves to be the most challenging case for all methods. AU-

TOSINDY achieves 70% recovery, significantly outperforming the 0% for Standard SINDy and 17% for Standard PySR. The bimodal distribution of outcomes, where trials either succeed completely ($R^2 \approx 1$) or fail catastrophically, is visible in Figure 6 as a large interquartile range shaded region for AUTOSINDY on the Duffing column. While Standard SINDy and Standard PySR fail in 8 and 7 out of 30 trials respectively, AUTOSINDY achieves zero simulation failures (see Section VC).

Finally, the Complex Lorenz system represents the most structurally challenging case, featuring a 3-dimensional chaotic attractor and a mixed polynomial-trigonometric coupling term. All methods show higher variance here, yet AUTOSINDY achieves zero simulation failures and a median complexity of 16, closely matching the ground truth of 15. Standard SINDy attains a marginally higher derivative R^2 of 0.992 versus 0.979 for AUTOSINDY, but this comes at the cost of $2.4\times$ the model complexity (see Section VD).

Full per-trial trajectory comparisons, state simulations, and phase portraits for all six systems are provided in Appendix B (Figs. 12–17).

C. Simulation Failure Analysis

Figure 7 presents the simulation failure analysis. The left heatmap shows hard integration failures (NaN, Inf, or early termination due to the divergence safety brake) per system. The right panel shows the aggregate mean failure rate trend as noise increases.

A critical finding from Figure 7 is that AUTOSINDY produces zero hard simulation crashes across all 180 trials. Standard SINDy produces hard failures in 4/30 harmonic oscillator trials, 6/30 Van der Pol trials, 8/30 Duffing trials, and 2/30 each for damped pendulum and modulated oscillator. Standard PySR crashes in 5/30 harmonic oscillator, 2/30 damped pendulum, and 7/30 Duffing trials.

The right panel of Figure 7 shows the aggregate failure trend with noise. While AUTOSINDY maintains a flat 0% crash rate at all levels, Standard SINDy rises steeply from $\sim 3\%$ at $\sigma = 0.01$ to $\sim 27\%$ at $\sigma = 0.05$, driven by increasingly bloated and unstable equation structures. Standard PySR rises to roughly 13% before plateauing, reflecting that its failures are more structurally determined than noise-determined.

The distinction between hard crashes (Figure 7) and simulation-tier failures (Figure 4) is important: AUTOSINDY’s 21.1% “Failed” ($R^2 < 0$) simulation tier consists entirely of

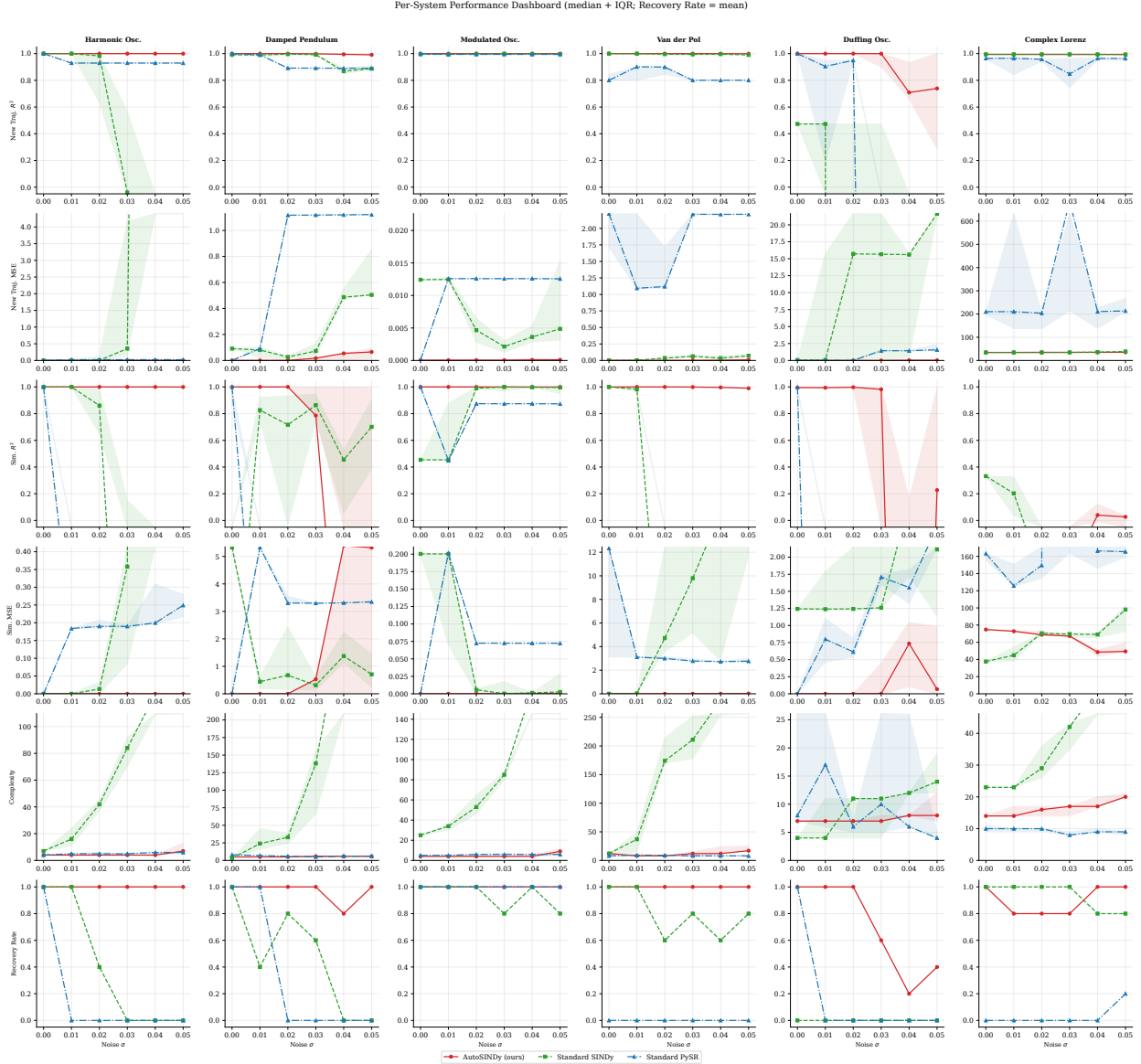


FIG. 6. Per-system performance dashboard. Each column corresponds to one of the six benchmark systems; each row shows one of six metrics as a function of noise level σ : validation-trajectory derivative R^2 , derivative MSE, simulation R^2 , simulation MSE, canonical complexity, and equation recovery rate ($R_{\text{val}}^2 \geq 0.99$). Solid lines indicate the median; shaded bands denote the interquartile range over five repeated trials. The bold dashed horizontal line in the complexity row indicates the ground-truth complexity of each system.

cases where the integration completed without crashing but the resulting trajectory was physically incorrect, which is a recoverable failure mode very different from the integration instabilities of the baselines.

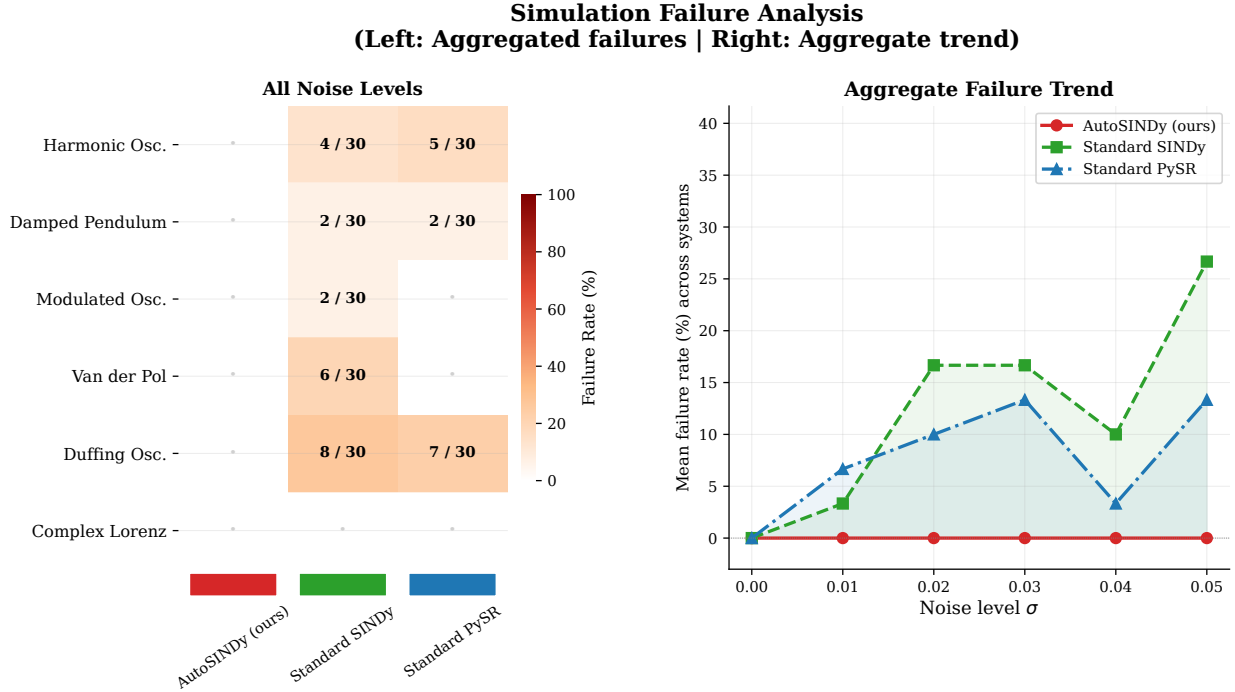


FIG. 7. Simulation failure analysis. **Left:** Heatmap of integration failure counts (out of 30 trials) per system and method. AUTOSINDY produces zero hard integration crashes across all systems and noise levels; Standard SINDy failures are concentrated on the Duffing oscillator (8/30) and Van der Pol (6/30); Standard PySR failures appear on the Duffing (7/30) and harmonic oscillator (5/30). **Right:** Mean failure rate trend vs. noise level, aggregated across systems. AUTOSINDY (red) remains at 0% throughout, while Standard SINDy (green) and Standard PySR (blue) rise sharply.

D. Model Parsimony

Figure 8 compares the median canonical complexity of the discovered equations against the ground-truth values (dashed line) for each system. AUTOSINDY recovers equations within 1–2 operators of the ground-truth complexity on all six systems. Standard SINDy’s enriched library induces dramatic over-complexity: 22.7 \times on Harmonic Oscillator, 14.8 \times on Damped Pendulum, 29.2 \times on Van der Pol, and 11.8 \times on Modulated Oscillator. The Van der Pol case is particularly striking: the true equation requires only 6 operations, but Standard SINDy discovers equations with a median of 175 operations, showing that while fitting the training data well, is far too complex to simulate stably and carries no interpretable physical

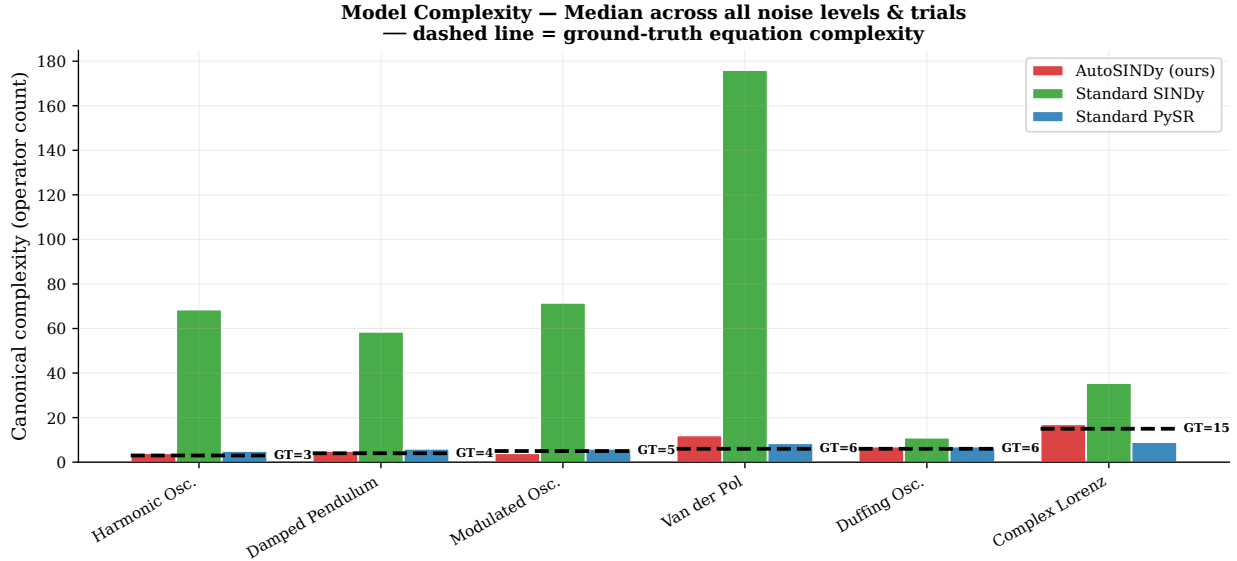


FIG. 8. Model complexity (median canonical operator count across all noise levels and trials). Dashed lines mark the ground-truth complexity of each system. AUTOSINDY (red) recovers near-ground-truth complexity on every system. Standard SINDy (green) is severely over-complex due to its large fixed polynomial-Fourier library. Standard PySR (blue) is often under-complex, indicating that standalone symbolic regression compresses equations at the cost of accuracy.

meaning. Standard PySR, by contrast, tends to under-compress (selecting low-complexity expressions from the Pareto front) at the cost of missing critical terms, which explains its superior parsimony scores alongside its poor simulation stability.

The error-vs.-complexity scatter plots (Figs. 9) confirm this picture across all systems simultaneously. AUTOSINDY’s trials cluster in the lower-left region of both plots, which means low complexity *and* low error, while Standard SINDy’s trials span a wide range of high complexities with no corresponding accuracy benefit, and Standard PySR’s trials show low complexity but substantially higher error.

E. Computational Efficiency

Figure 10 shows wall-clock discovery and simulation times as boxplots per system. AUTOSINDY and Standard PySR incur comparable discovery overheads (~ 20 – 40 s, median ~ 24 s and ~ 20 s respectively) reflecting that both invoke the same PYSR engine. Standard SINDy requires under 1 s for library fitting. The discovery overhead of AUTOSINDY is

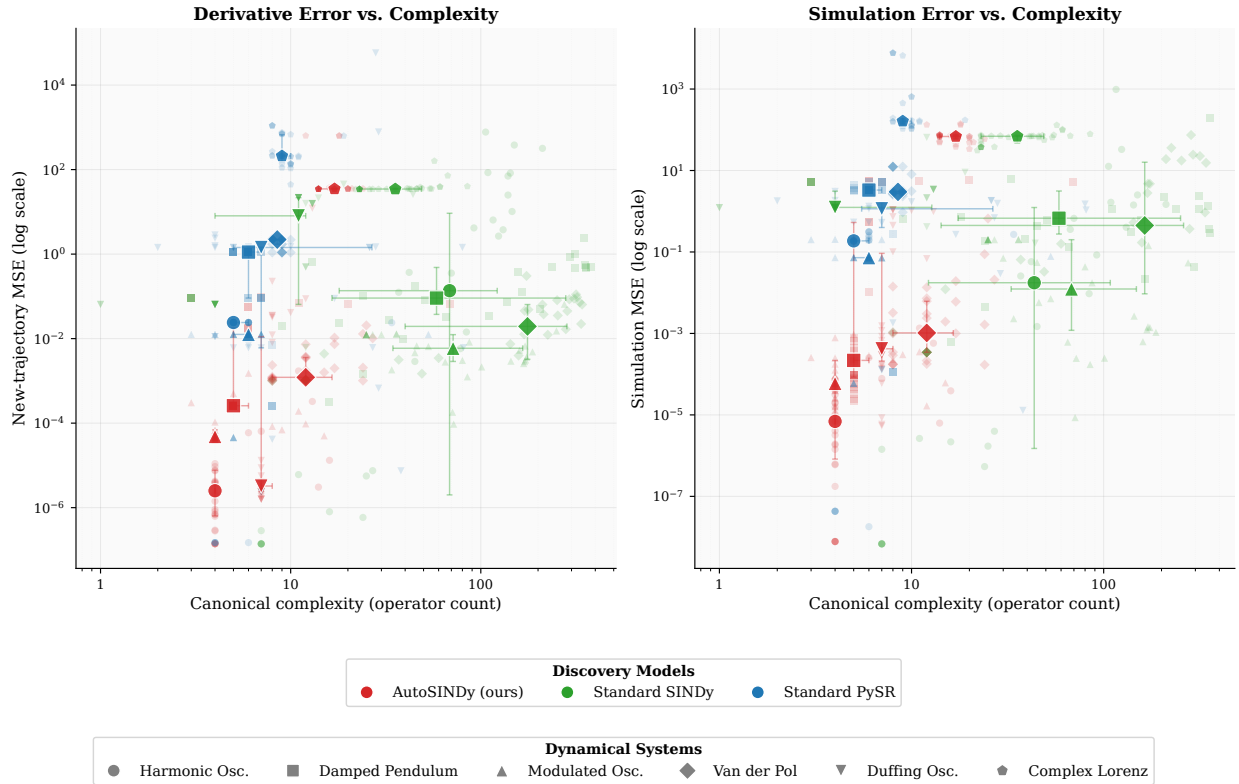


FIG. 9. Scatter plots comparing canonical model complexity against prediction error (Derivative MSE and Simulation MSE) on a logarithmic scale. Both panels use shared color encodings for the discovery algorithms and distinct marker shapes for the underlying dynamical systems. Solid markers with error bars denote the median performance and interquartile ranges, while faded background markers represent individual trial runs. AUTOSINDY consistently occupies the lower-left region, combining low complexity with low error.

therefore the cost of automation: it replaces the manual feature-engineering step with a systematic search.

Importantly, AUTOSINDY is consistently the *fastest* method for simulation across all systems, with a tight distribution concentrated below 2 s (median ~ 1.2 s). Standard SINDy’s simulation time is highly variable, including outliers exceeding 10^2 s, driven by numerically stiff ODE systems arising from its bloated coefficient structures. Standard PySR shows the highest and most variable simulation times (~ 5 – 20 s, with extreme outliers), consistent with complex expression trees and frequent near-divergent trajectories that require small integrator steps.

The compact equations recovered by AUTOSINDY therefore provide a compounding ad-

Computation Time Distributions (Box Plot / Log Scale)

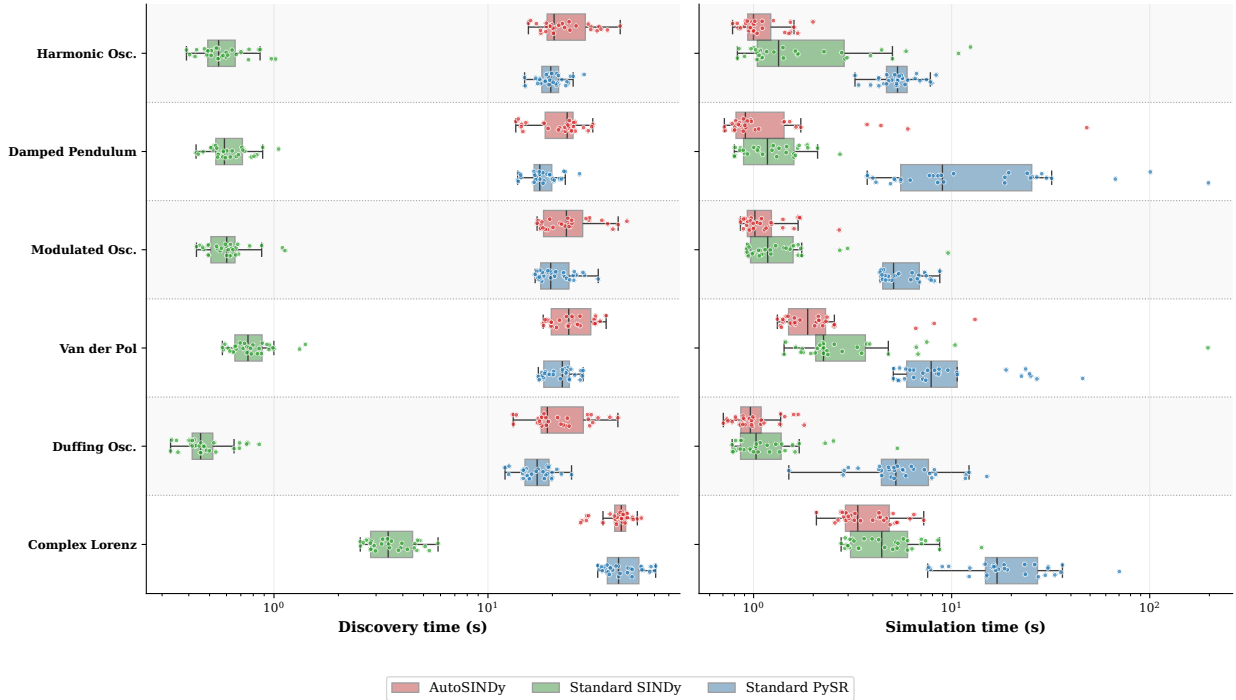


FIG. 10. Computation time distributions for discovery (left) and simulation (right). Both axes use logarithmic scale. AUTOSINDY’s discovery time (10–30s) is comparable to or slightly higher than standalone Standard PySR, and roughly 10–30× longer than Standard SINDy, which does not require symbolic search. Simulation times for AUTOSINDY are uniformly short and low-variance due to the compactness of the discovered equations; Standard SINDy and Standard PySR exhibit higher and more variable simulation times.

vantage: they are not only more interpretable but also substantially cheaper to simulate, which is a property of direct practical value in real-time or embedded applications.

F. Summary of Quantitative Results

Table II presents a comprehensive performance breakdown of AutoSINDy compared to standard baseline methods across six canonical dynamical systems. To evaluate robustness against observational noise and varying initial conditions, we report the median metrics (and mean Recovery Rate) aggregated across all noise levels and random seeds. The evaluation encompasses structural discovery accuracy (Derivative R^2 and MSE), long-term integration

stability (Simulation R^2 and MSE), model parsimony (Canonical Complexity), and the overall equation Recovery Rate.

As demonstrated in Table II, AutoSINDy consistently outperforms the baselines, maintaining near-perfect predictive accuracy (Derivative $R^2 \approx 1.0$) and stable forward simulation (Simulation $R^2 \approx 1.0$) across the majority of the evaluated systems. Furthermore, AutoSINDy successfully avoids equation bloat, consistently discovering parsimonious models whose canonical complexity perfectly or closely matches the ground truth.

In contrast, Standard SINDy frequently suffers from catastrophic simulation divergence (evidenced by severely negative Simulation R^2 scores and inflated Simulation MSE), even in cases where it achieves reasonable derivative approximations. Meanwhile, Standard PySR struggles significantly with both forward simulation stability and structural recovery, often yielding low recovery rates. These results underscore the efficacy of AutoSINDy’s hybrid discovery-then-solve framework in identifying equations that are not only structurally accurate but also dynamically stable over long time horizons.

VI. DISCUSSION

A. Why AUTOSINDY Outperforms Its Components in Isolation

The performance gap between AUTOSINDY and its two individual components, PYSR alone and SINDY alone, is instructive. Standard PySR achieves 28.3% Excellent derivative performance (Figure 4) and collapses to 8.3% in simulation. This discrepancy traces to the lack of regularization: without a sparsity-promoting mechanism, genetic programming optimizes fit on observed training chunks, where even slightly incorrect coefficient values produce models that diverge over long integration horizons. Particularly telling is the 0% recovery on the Van der Pol oscillator: PySR consistently identifies $x_0^2 x_1$ as a relevant term, but its estimated coefficient deviates from the true value by a margin that accumulates into trajectory divergence.

Standard SINDy suffers from two distinct failure modes depending on the relationship between its fixed library and the true governing structure. The first is *over-completeness under noise*: the polynomial-Fourier basis contains the correct terms for most systems (e.g., $x_0^2 x_1$ for Van der Pol, $\sin(x_0)$ for the damped pendulum), but also hundreds of correlated

TABLE II. Aggregated Performance by System. Reported are median values (mean for Recovery %). Bold indicates the best performing model per system.

System	Model	Deriv. R^2	Sim. R^2	Deriv. MSE	Sim. MSE	Comp.	Recov.
Harmonic Osc.	AutoSINDy (ours)	1.000	1.000	2.51e-06	6.93e-06	4.0	100.0%
	Standard SINDy	0.600	0.272	0.136	0.071	68.5	40.0%
	Standard PySR	0.929	-0.928	0.024	0.191	5.0	16.7%
Damped Pendulum	AutoSINDy (ours)	1.000	1.000	2.58e-04	2.18e-04	5.0	96.7%
	Standard SINDy	0.989	0.622	0.091	0.912	58.5	46.7%
	Standard PySR	0.891	-0.497	1.117	3.315	6.0	33.3%
Modulated Osc.	AutoSINDy (ours)	1.000	1.000	4.84e-05	5.95e-05	4.0	100.0%
	Standard SINDy	0.997	0.946	5.91e-03	0.030	71.5	93.3%
	Standard PySR	0.994	0.874	0.013	0.072	6.0	100.0%
Van der Pol	AutoSINDy (ours)	1.000	0.999	1.21e-03	1.03e-03	12.0	100.0%
	Standard SINDy	0.997	-0.724	0.019	3.761	176.0	80.0%
	Standard PySR	0.801	-0.516	2.212	2.991	8.5	0.0%
Duffing Osc.	AutoSINDy (ours)	1.000	0.993	3.25e-06	4.21e-04	7.0	70.0%
	Standard SINDy	-64.794	-6.061	8.053	2.136	11.0	0.0%
	Standard PySR	-10.721	-5.884	1.435	1.410	7.0	16.7%
Complex Lorenz	AutoSINDy (ours)	0.994	-0.388	34.905	68.455	17.0	90.0%
	Standard SINDy	0.994	-0.357	34.644	69.153	35.5	93.3%
	Standard PySR	0.962	-1.982	210.237	163.040	9.0	3.3%

alternatives. Under noisy derivative estimates, the optimizer distributes coefficients across these spurious terms rather than concentrating them on the few correct ones, producing the catastrophic equation bloat visible in Figure 8: 69 operators for the harmonic oscillator against a ground truth of 3, and 59 for the damped pendulum against a ground truth of 4. The second failure mode is *genuine structural incompleteness*: the `FourierLibrary` applies \sin / \cos to individual state variables only, so the compound term $x_1 \sin(x_0 + x_2)$ in the Complex Lorenz system is genuinely absent. SINDy approximates it with many polynomial-Fourier cross-products, explaining simultaneously its deceptively high 93% recovery rate and

its 39-operator complexity against a ground truth of 15.

AUTOSINDY resolves both failure modes by construction. The DISCOVER stage actively mines for the system-specific functional forms present in the data, including non-standard compound terms such as $x_1 \sin(x_0 + x_2)$, rather than assuming they belong to a fixed class. The CURATE stage then eliminates over-completeness by pruning the discovered pool to a compact, non-redundant basis before any regression is performed.

B. The Critical Role of Library Curation

The curation stage is not merely a preprocessing convenience; it is a necessary condition for well-conditioned sparse regression. Without collinearity pruning, Θ can be near-singular. For example, after PySR discovers both $x_0 \sin(x_1)$ and $x_0 \cos(x_1)$ as candidates, these two features are highly correlated over much of the attractor, and including both destabilizes STLSQ coefficient estimation. By rejecting any candidate whose correlation with already-accepted terms exceeds a threshold, the curation pipeline guarantees that every admitted term carries genuinely independent predictive information.

The simplicity bias, which is sorting candidates in ascending order of SymPy operator count before applying the correlation filter, is what makes this pruning meaningful rather than arbitrary. By always admitting the simplest expression that captures a given piece of information, the curation algorithm directly implements a form of Occam’s razor. Complex terms are rejected not because they are wrong, but because a simpler term already explains the same variance in the data. Empirically, this produces libraries that are minimally sufficient and containing the correct functional forms without redundant decorations. Therefore, the downstream STLSQ optimizer can then concentrate all coefficient mass on the small number of genuinely active terms.

C. Simulation Stability as a Test of Physical Validity

The zero hard-crash rate of AUTOSINDY across all 180 trials (Figure 7) is a substantive finding rather than a secondary observation. An integration crash, where state variables diverge to infinity within the simulation window, indicates that the discovered model assigns arbitrarily large derivatives to reachable states. This is not merely numerical inaccuracy;

it reflects a physically incoherent equation structure in which the right-hand side of the ODE grows without bound. Standard SINDy produces hard crashes in 8/30 Duffing, 6/30 Van der Pol, 4/30 harmonic oscillator, and 2/30 each of damped pendulum and modulated oscillator trials. Standard PySR crashes in 7/30 Duffing and 5/30 harmonic oscillator trials.

The aggregate failure trend in Figure 7 (right panel) reveals an important distinction: Standard SINDy’s crash rate *increases sharply with noise*, reaching $\sim 27\%$ at $\sigma = 0.05$, while Standard PySR’s rate stabilizes around 13% and is largely noise-independent. This reflects the different origins of the two failure modes. SINDy crashes are induced by noise inflating the derivative estimates and causing the over-complete optimizer to assign destabilizing coefficients to high-degree terms; this mechanism worsens as noise grows. PySR crashes arise from coefficient imprecision that is structurally determined by the symbolic search rather than by noise level, which is why the rate does not grow systematically with σ . AUTOSINDY’s consistent avoidance of hard crashes across all 180 trials and all six systems confirms that the discovered equations, whatever their coefficient errors, remain within a plausible physical manifold.

D. The Duffing Oscillator: Limits of Noise Robustness

The Duffing oscillator ($\dot{x}_1 = -\delta x_1 - \alpha x_0 - \beta x_0^3$) exposes a fundamental boundary of the current framework. Its bistable potential ($\alpha < 0, \beta > 0$) concentrates trajectory density near the two equilibria, where the derivative of x_0^3 is largest and most sensitive to noise. Under moderate noise, all three methods struggle: AUTOSINDY achieves 70% recovery (vs. 0% for Standard SINDy and 17% for PySR), but the remaining 30% of trials produce incorrect coefficient signs. The per-system dashboard (Figure 6, Duffing column) shows that AUTOSINDY’s simulation R^2 transitions sharply from near-perfect to failed without a gradual intermediate regime, reflecting the binary nature of whether the correct x_0^3 coefficient sign is identified.

E. Parsimony, Interpretability, and Downstream Scientific Value

Figure 8 demonstrates that AUTOSINDY consistently produces equations within a narrow margin of the true ground-truth complexity. This parsimony is not merely an aesthetic

preference; it has concrete practical consequences.

Discovered equations at $1.21\times$ the ground-truth complexity can be directly submitted to downstream scientific analysis. For a dynamical system described by 4 or 6 operators, an analyst can compute equilibria analytically, perform linearization and stability analysis, derive conservation laws, apply perturbation theory, or use the equation as a mechanistic prior in a downstream Bayesian model. None of these operations is tractable on a Van der Pol model with 173 operators or a harmonic oscillator model with 69 operators, even if their derivative prediction scores are nominally acceptable.

The timing results (Figure 10) make the same point in computational terms. AUTOSINDY is systematically the fastest method for simulation. This is not because of any algorithmic optimization of the integrator, but because its discovered equations have fewer right-hand-side operations per step, producing less stiff ODE systems that the Radau solver can traverse with larger time steps. Standard SINDy’s bloated equations, by contrast, frequently produce ODE systems whose stiffness requires extremely fine time-stepping, explaining the outliers reaching 10^2 s in Figure 10 (right column) even on two-dimensional systems like the harmonic oscillator.

The contrast between derivative R^2 and simulation speed therefore captures a key insight that the prediction accuracy on observed states is a necessary but insufficient criterion for equation quality. A concise, physically coherent equation is simultaneously more accurate, more stable, more interpretable, and faster to simulate than a bloated approximation with a comparable short-horizon fit. AUTOSINDY demonstrates that these desiderata can be jointly optimized through principled basis construction rather than requiring a post-hoc trade-off.

F. Limitations and Future Work

Several limitations of the current framework merit acknowledgment.

a. Computational cost. AUTOSINDY’s discovery time (10–30s per state variable) is moderate for two- and three-dimensional systems but scales linearly in the number of state variables and chunks, which could become prohibitive for high-dimensional systems. Promising mitigation strategies include: amortized symbolic regression (pre-training a surrogate to predict candidate terms from data statistics), parallel PYSR calls per state variable, and

warm-starting from libraries curated on related systems.

b. Chaotic long-horizon simulation. The Complex Lorenz simulation results confirm that recovering correct governing equations does not guarantee accurate long-horizon simulation for chaotic systems. Chaotic sensitivity means any integration error compounds exponentially; even the true model with finite-precision arithmetic will diverge from a specific reference trajectory. Future evaluation should use attractor-geometry metrics that are insensitive to phase shifts.

c. Extension to PDEs and real data. All experiments use synthetic ODE data with controlled Gaussian noise. Extension to partial differential equations would require spatially local symbolic regression on data slices, followed by global library curation enforcing spatial consistency. Applying AUTOSINDY to real experimental time series, where the ground truth is unknown, data may be irregular, and state variables may be partially observed, remains a high-priority validation direction and a natural next step given the framework’s noise robustness demonstrated here.

VII. CONCLUSION

We have presented AUTOSINDY, a hybrid discovery-then-solve framework that automates the feature-engineering bottleneck in the sparse identification of nonlinear dynamical systems. By using PYSR-based symbolic regression as an unsupervised basis mining tool, coupling it with a principled collinearity-aware curation pipeline, and feeding the resulting custom library into SINDY’s robust sparse optimizers, AUTOSINDY recovers correct governing equations from noisy data without requiring any prior specification of the mathematical form. Benchmarks across canonical nonlinear systems demonstrate consistent advantages in equation accuracy, trajectory generalization, and symbolic parsimony. Unlike the large, black-box coefficient matrices produced by enriched SINDY libraries or the point-estimate expressions of standalone symbolic regression, the compact equations produced by AUTOSINDY are immediately usable for mechanistic interpretation, control design, and hypothesis generation. Ultimately, this work establishes a scalable pathway for automated scientific discovery in domains where the governing mathematics is genuinely unknown, including systems biology, neuroscience, climate modeling, and materials science. The complete source code, experimental configurations, and benchmark scripts are publicly available

at <https://github.com/mabasiri95/AutoSINDy>.

- [1] G. Camps-Valls, A. Gerhardus, U. Ninad, G. Varando, G. Martius, E. Balaguer-Ballester, R. Vinuesa, E. Diaz, L. Zanna, and J. Runge, [Discovering causal relations and equations from data](#) (2023), [arXiv:2305.13341 \[physics.data-an\]](#).
- [2] H. Wang, T. Fu, Y. Du, W. Gao, K. Huang, Z. Liu, P. Chandak, S. Liu, P. Van Katwyk, A. Deac, A. Anandkumar, K. Bergen, C. P. Gomes, S. Ho, P. Kohli, J. Lasenby, J. Leskovec, T.-Y. Liu, A. Manrai, D. Marks, B. Ramsundar, L. Song, J. Sun, J. Tang, P. Veličković, M. Welling, L. Zhang, C. W. Coley, Y. Bengio, and M. Zitnik, Scientific discovery in the age of artificial intelligence, [Nature](#) **620**, 47 (2023).
- [3] J. N. Kutz, P. Battaglia, M. Brenner, K. Carlberg, A. Hagberg, S. Ho, S. Hoyer, H. Lange, H. Lipson, M. W. Mahoney, F. Noe, M. Welling, L. Zanna, F. Zhu, and S. L. Brunton, [Accelerating scientific discovery with the common task framework](#) (2025), [arXiv:2511.04001 \[cs.LG\]](#).
- [4] J. L. Callahan, S. L. Brunton, and J.-C. Loiseau, On the role of nonlinear correlations in reduced-order modelling, [Journal of Fluid Mechanics](#) **938**, A1 (2022).
- [5] E. P. Alves and F. Fiuza, Data-driven discovery of reduced plasma physics models from fully kinetic simulations, [Phys. Rev. Res.](#) **4**, 033192 (2022).
- [6] L. Zanna and T. Bolton, Data-driven equation discovery of ocean mesoscale closures, [Geophysical Research Letters](#) **47**, e2020GL088376 (2020), e2020GL088376 10.1029/2020GL088376, <https://agupubs.onlinelibrary.wiley.com/doi/pdf/10.1029/2020GL088376>.
- [7] M. Brenner, F. Hess, J. M. Mikhaeil, L. Bereska, Z. Monfared, P.-C. Kuo, and D. Durstewitz, [Tractable dendritic rnns for reconstructing nonlinear dynamical systems](#) (2022), [arXiv:2207.02542 \[cs.LG\]](#).
- [8] C. Métayer, A. Ballesta, and J. Martinelli, Data-driven discovery of digital twins in biomedical research, [Briefings in Bioinformatics](#) **27**, bbaf722 (2026), <https://academic.oup.com/bib/article-pdf/27/1/bbaf722/66846059/bbaf722.pdf>.
- [9] S. L. Brunton, J. L. Proctor, and J. N. Kutz, Discovering governing equations from data by sparse identification of nonlinear dynamical systems, [Proceedings of the National Academy of Sciences](#) **113**, 3932 (2016), <https://www.pnas.org/doi/pdf/10.1073/pnas.1517384113>.

- [10] S. H. Rudy, S. L. Brunton, J. L. Proctor, and J. N. Kutz, Data-driven discovery of partial differential equations, *Science Advances* **3**, e1602614 (2017), <https://www.science.org/doi/pdf/10.1126/sciadv.1602614>.
- [11] B. M. de Silva, K. Champion, M. Quade, J.-C. Loiseau, J. N. Kutz, and S. L. Brunton, Pysindy: A python package for the sparse identification of nonlinear dynamical systems from data, *Journal of Open Source Software* **5**, 2104 (2020).
- [12] A. A. Kaptanoglu, B. M. de Silva, U. Fasel, K. Kaheman, A. J. Goldschmidt, J. Callahan, C. B. Delahunt, Z. G. Nicolaou, K. Champion, J.-C. Loiseau, J. N. Kutz, and S. L. Brunton, Pysindy: A comprehensive python package for robust sparse system identification, *Journal of Open Source Software* **7**, 3994 (2022).
- [13] S. L. Brunton, J. L. Proctor, and J. N. Kutz, Sparse identification of nonlinear dynamics with control (SINDYc), *IFAC-PapersOnLine* **49**, 710 (2016), 10th IFAC Symposium on Nonlinear Control Systems NOLCOS 2016.
- [14] K. Kaheman, J. N. Kutz, and S. L. Brunton, Sindy-pi: a robust algorithm for parallel implicit sparse identification of nonlinear dynamics, *Proceedings of the Royal Society A: Mathematical, Physical and Engineering Sciences* **476**, 20200279 (2020), <https://royalsocietypublishing.org/rspa/article-pdf/doi/10.1098/rspa.2020.0279/638633/rspa.2020.0279.pdf>.
- [15] K. Champion, B. Lusch, J. N. Kutz, and S. L. Brunton, Data-driven discovery of coordinates and governing equations, *Proceedings of the National Academy of Sciences* **116**, 22445 (2019), <https://www.pnas.org/doi/pdf/10.1073/pnas.1906995116>.
- [16] K. Champion, P. Zheng, A. Y. Aravkin, S. L. Brunton, and J. N. Kutz, A unified sparse optimization framework to learn parsimonious physics-informed models from data, *IEEE Access* **8**, 169259 (2020).
- [17] D. A. Messenger and D. M. Bortz, Weak sindy for partial differential equations, *Journal of Computational Physics* **443**, 110525 (2021).
- [18] N. M. Mangan, J. N. Kutz, S. L. Brunton, and J. L. Proctor, Model selection for dynamical systems via sparse regression and information criteria, *Proceedings of the Royal Society A: Mathematical, Physical and Engineering Sciences* **473**, 20170009 (2017), <https://royalsocietypublishing.org/rspa/article-pdf/doi/10.1098/rspa.2017.0009/365284/rspa.2017.0009.pdf>.

- [19] U. Fasel, J. N. Kutz, B. W. Brunton, and S. L. Brunton, Ensemble-sindy: Robust sparse model discovery in the low-data, high-noise limit, with active learning and control, *Proceedings of the Royal Society A: Mathematical, Physical and Engineering Sciences* **478**, 20210904 (2022), <https://royalsocietypublishing.org/rspa/article-pdf/doi/10.1098/rspa.2021.0904/355985/rspa.2021.0904.pdf>.
- [20] J. R. Koza, *Genetic Programming: On the Programming of Computers by Means of Natural Selection* (MIT Press, Cambridge, MA, 1992).
- [21] M. Schmidt and H. Lipson, Distilling free-form natural laws from experimental data, *Science* **324**, 81 (2009), <https://www.science.org/doi/pdf/10.1126/science.1165893>.
- [22] M. Cranmer, *Interpretable machine learning for science with pysr and symbolicregression.jl* (2023), [arXiv:2305.01582 \[astro-ph.IM\]](https://arxiv.org/abs/2305.01582).
- [23] B. R. Brum, L. Lober, I. Previdelli, and F. A. Rodrigues, Discovering equations from data: symbolic regression in dynamical systems, *Journal of Physics: Complexity* **7**, 012001 (2026).
- [24] X. Dong, Y.-L. Bai, Y. Lu, and M. Fan, An improved sparse identification of nonlinear dynamics with akaike information criterion and group sparsity, *Nonlinear Dynamics* **111**, 1485 (2023).
- [25] S. M. Hirsh, D. A. Barajas-Solano, and J. N. Kutz, Sparsifying priors for bayesian uncertainty quantification in model discovery, *Royal Society Open Science* **9**, 211823 (2022), <https://royalsocietypublishing.org/rsos/article-pdf/doi/10.1098/rsos.211823/994951/rsos.211823.pdf>.
- [26] M. Virgolin and S. P. Pissis, *Symbolic regression is np-hard* (2022), [arXiv:2207.01018 \[cs.NE\]](https://arxiv.org/abs/2207.01018).
- [27] S. L. Brunton, B. W. Brunton, J. L. Proctor, E. Kaiser, and J. N. Kutz, Chaos as an intermittently forced linear system, *Nature Communications* **8**, 19 (2017).
- [28] S. H. Rudy, J. Nathan Kutz, and S. L. Brunton, Deep learning of dynamics and signal-noise decomposition with time-stepping constraints, *Journal of Computational Physics* **396**, 483 (2019).
- [29] M. Raissi, P. Perdikaris, and G. Karniadakis, Physics-informed neural networks: A deep learning framework for solving forward and inverse problems involving nonlinear partial differential equations, *Journal of Computational Physics* **378**, 686 (2019).
- [30] R. T. Q. Chen, Y. Rubanova, J. Bettencourt, and D. K. Duvenaud, Neural ordinary differential equations, in *Advances in Neural Information Processing Systems*, Vol. 31, edited by S. Bengio,

- H. Wallach, H. Larochelle, K. Grauman, N. Cesa-Bianchi, and R. Garnett (Curran Associates, Inc., 2018).
- [31] S. d’Ascoli, S. Becker, A. Mathis, P. Schwaller, and N. Kilbertus, [Odeformer: Symbolic regression of dynamical systems with transformers](#) (2023), [arXiv:2310.05573 \[cs.LG\]](#).
- [32] A. Meurer, C. P. Smith, M. Paprocki, O. Čertík, S. B. Kirpichev, M. Rocklin, A. Kumar, S. Ivanov, J. K. Moore, S. Singh, T. Rathnayake, S. Vig, B. E. Granger, R. P. Muller, F. Bonazzi, H. Gupta, S. Vats, F. Johansson, F. Pedregosa, M. J. Curry, A. R. Terrel, v. Roučka, A. Saboo, I. Fernando, S. Kulal, R. Cimrman, and A. Scopatz, Sympy: symbolic computing in python, [PeerJ Computer Science](#) **3**, e103 (2017).

Appendix A: Effect of Noise on Raw Signal Quality

This appendix supplements Sec. [IV B](#) of the main text. Figure [11](#) illustrates how the noise level σ affects the raw input data available to all methods. The left columns show the state trajectories x_1 and x_2 , which remain visually smooth even at high noise because noise is injected additively on the state. The centre columns show the numerically estimated time derivatives \dot{x}_1 and \dot{x}_2 , which serve as the regression targets for all SINDY-based methods and which degrade sharply with noise: at $\sigma = 0.05$, the derivative signal is almost entirely obscured. The right column shows the corresponding phase-space trajectory; the flow arrows become increasingly erratic as noise grows, reflecting the corrupted derivative estimates.

Appendix B: Per-System Identification Results

This appendix supplements Sec. [V B](#) of the main text. Figures [12–17](#) show representative single-trial identification results for each of the six benchmark systems. For each system, we show: (i) derivative fits on the training/test trajectory, (ii) generalization to an unseen trajectory, (iii) state-variable simulation comparison, and (iv) phase portrait. Each figure follows the same layout. The left panels show derivative comparisons on the training/test trajectory which vertical dashed lines mark the training window boundaries (upper left), and an independent out-of-sample unseen trajectory (lower left). The upper right panel shows forward-simulated state variables from a held-out initial condition over time compared against the ground truth. The lower right panel shows the phase portrait comparing the

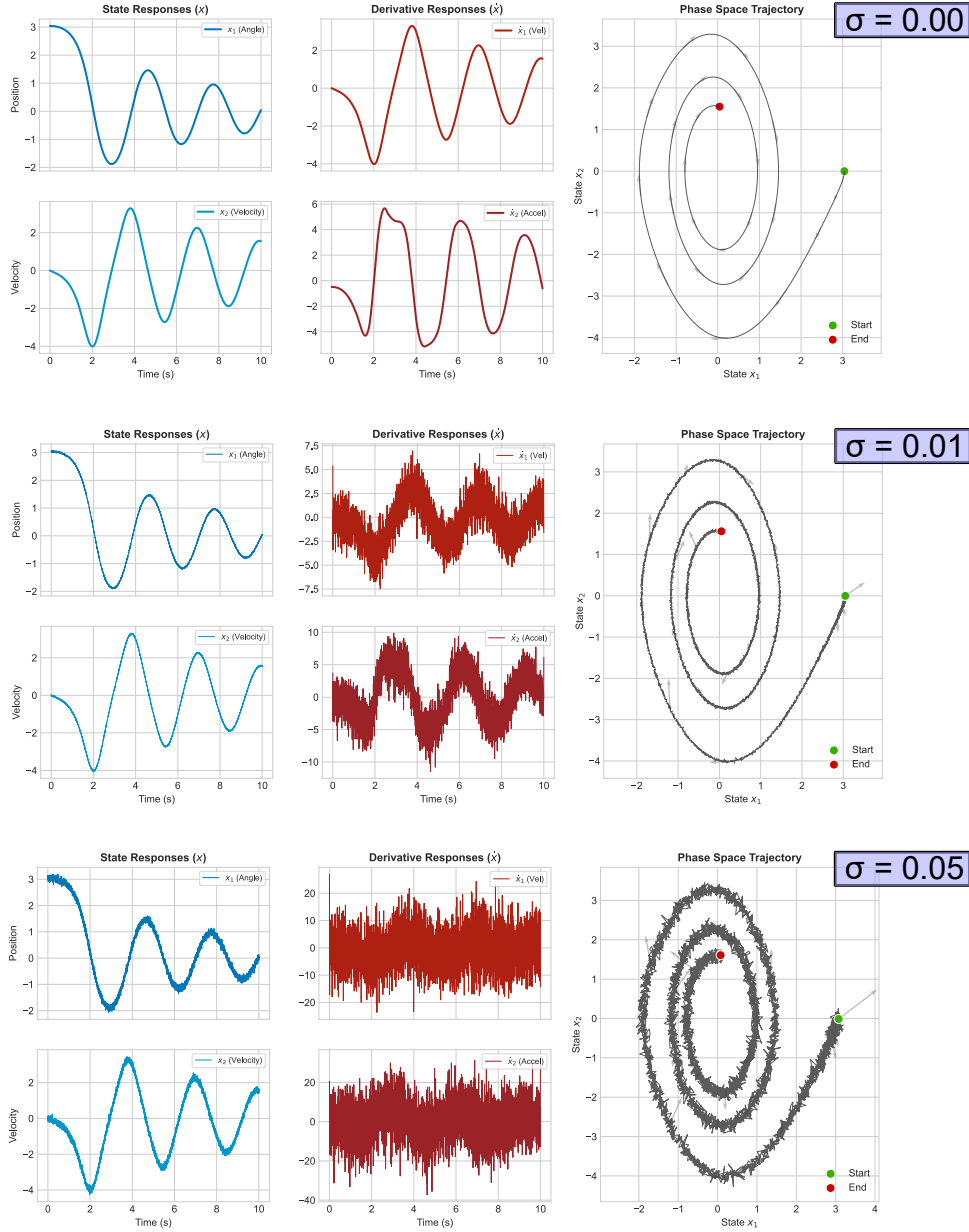


FIG. 11. Effect of measurement noise on system observability. State responses (x , left column), numerical derivative estimates (\dot{x} , center column), and phase-space trajectories (right column) for the damped pendulum at three noise levels: $\sigma = 0.00$ (top), $\sigma = 0.01$ (middle), and $\sigma = 0.05$ (bottom). While the state signals remain interpretable across all noise levels, the derivative estimates degrade rapidly, and the phase portrait becomes densely cluttered.

predicted dynamics against the true underlying model. AUTOSINDY (red dashed), Standard SINDY (green dotted), and Standard PYSR (blue dash-dot) are compared against the true underlying model (gray solid).

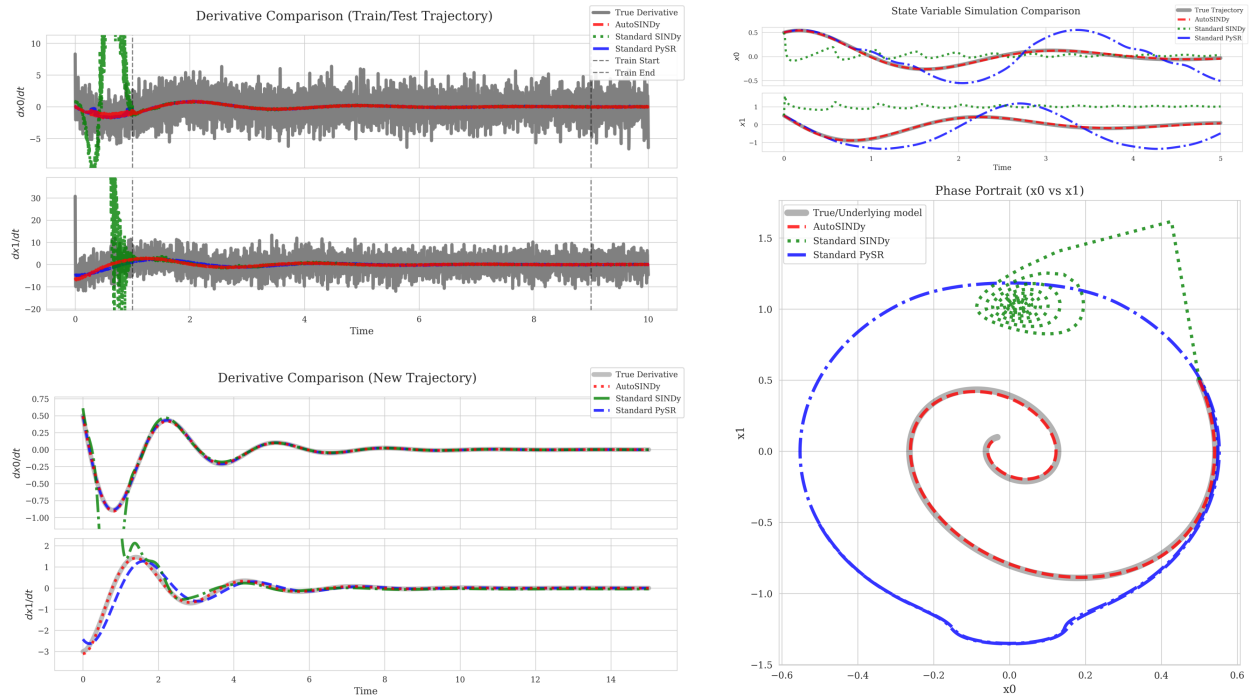


FIG. 12. Identification results for the **harmonic oscillator** ($\dot{x}_0 = x_1$, $\dot{x}_1 = -k_1x_0 - k_2x_1$) at $\sigma = 0.08$. AUTO-SINDY recovers the true dynamics and maintains near-perfect concentric-circle phase portrait structure. Standard SINDY fails to generalize to the data beyond the training window boundaries and exhibits trajectory drift due to library bloat (median complexity ≈ 69). Also, standard PYSR produces a limit-cycle-like divergence in the phase portrait, indicating a missed damping term.

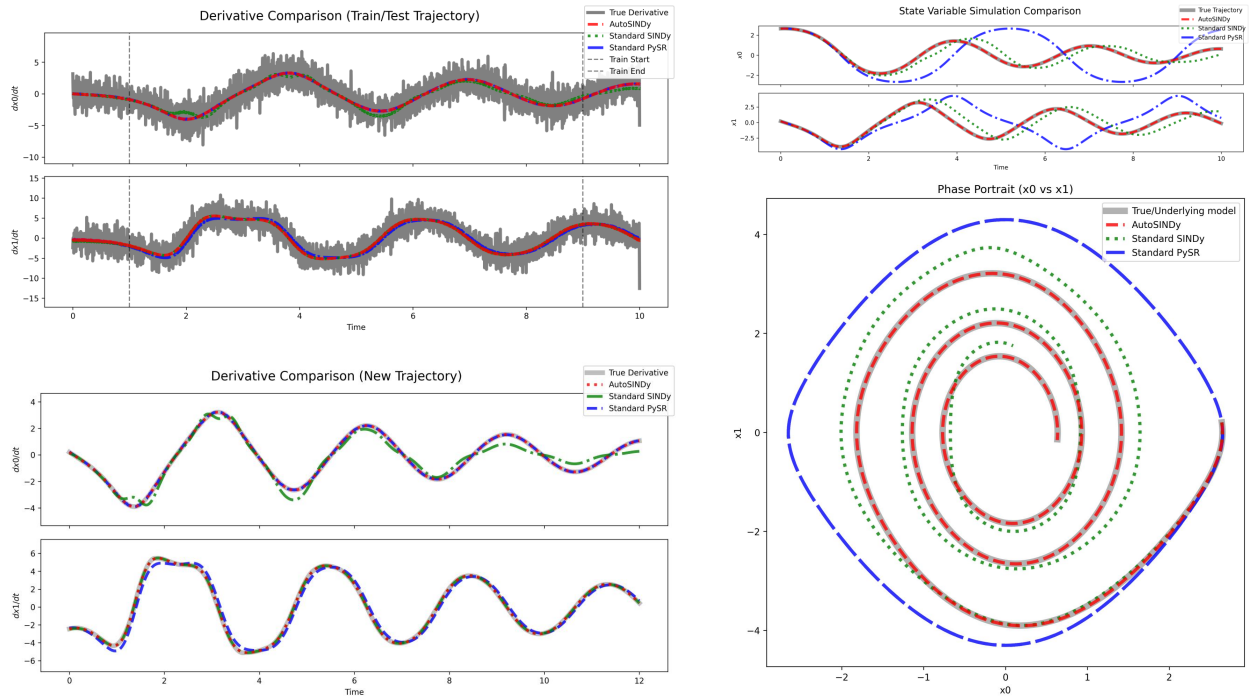


FIG. 13. Identification results for the **damped pendulum** ($\dot{x}_0 = x_1$, $\dot{x}_1 = -bx_1 - c \sin(x_0)$) at $\sigma = 0.01$. AUTO SINDY correctly recovers the nonlinearity and reproduces the inward-spiralling phase portrait with near-zero simulation error. Standard SINDY retains numerous spurious polynomial–Fourier cross-terms (median complexity ≈ 59), degrading simulation fidelity. Standard PYSR misidentifies the coefficient of the damping term, causing the trajectory not to decay.

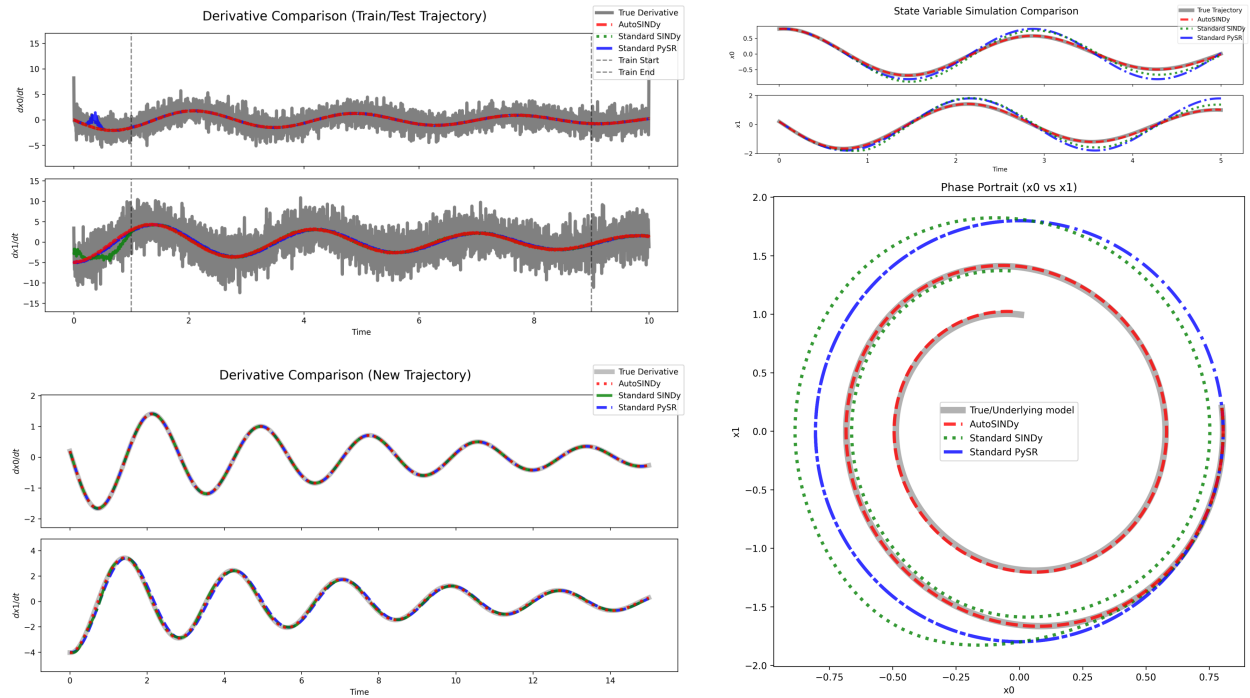


FIG. 14. Identification results for the **modulated oscillator** ($\dot{x}_0 = x_1$, $\dot{x}_1 = -bx_1 \cos(x_0) - kx_0$) at $\sigma = 0.03$. AUTOSINDY recovers the damping behavior and produces a stable decaying-oscillation trajectory. Both baselines fail to identify the exact dynamics, resulting in errors in both the derivative comparison beyond the training data and in the phase portrait trajectories.

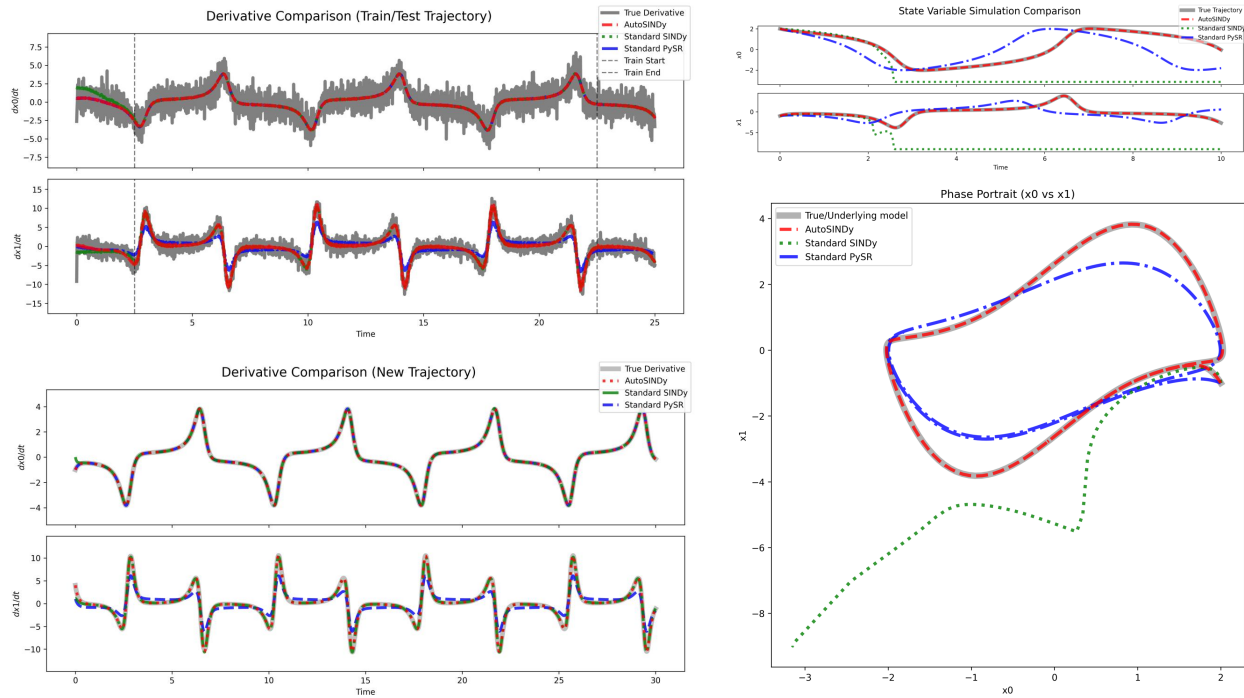


FIG. 15. Identification results for the **Van der Pol oscillator** ($\dot{x}_0 = x_1$, $\dot{x}_1 = \mu(1 - x_0^2)x_1 - x_0$) at $\sigma = 0.02$. AUTOSINDY recovers the limit-cycle structure and the correct dynamics, yielding a stable phase portrait. Standard SINDY's bloated equations (median complexity ≈ 175) causing trajectory divergence. Standard PYSR consistently misestimates the accurate dynamics, producing different limit cycles.

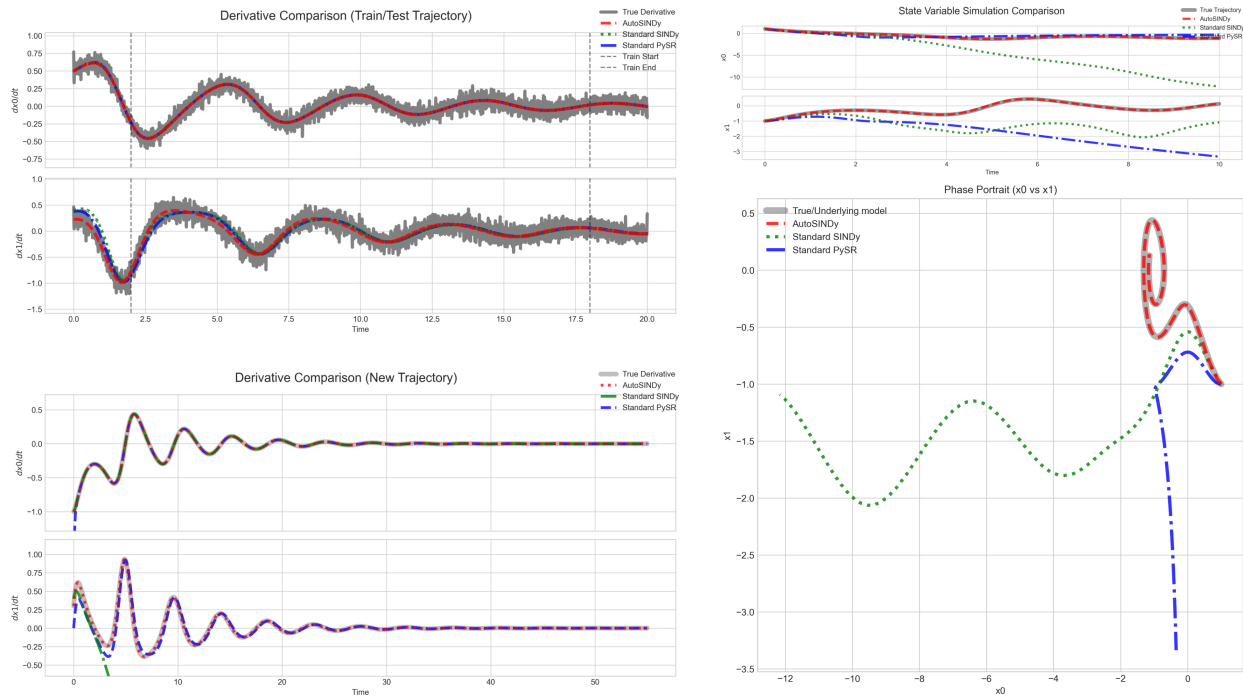


FIG. 16. Identification results for the **Duffing oscillator** ($\dot{x}_0 = x_1$, $\dot{x}_1 = -\delta x_1 - \alpha x_0 - \beta x_0^3$) at $\sigma = 0.05$. This is the most challenging system for all methods due to the bistable potential and high derivative sensitivity near the equilibria. AUTOSINDY recovered the true dynamics and the phase portrait closely matches the true trajectory.

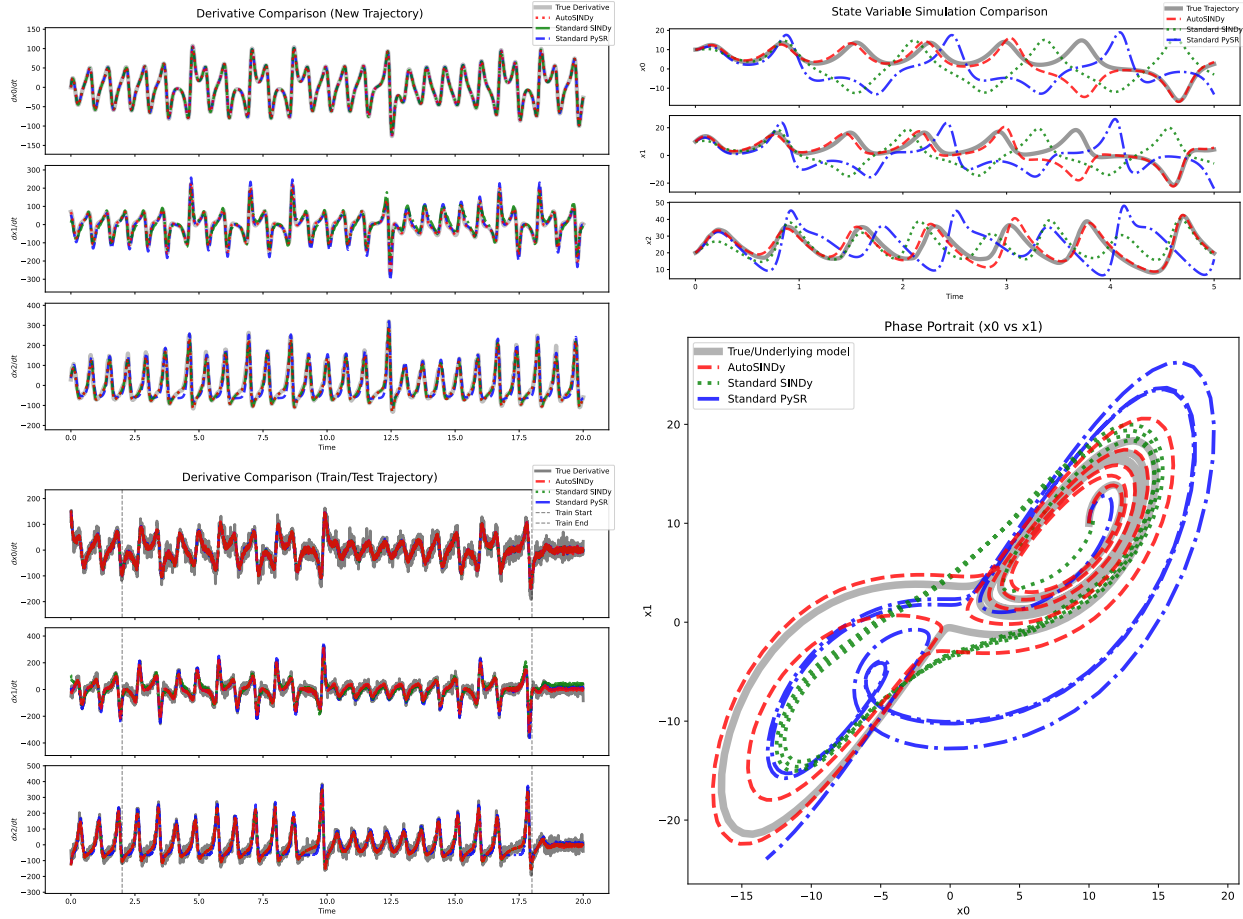


FIG. 17. Identification results for the **Complex Lorenz system** ($\dot{x}_0 = \sigma(x_1 - x_0)$, $\dot{x}_1 = x_0(\rho - x_2) - x_1$, $\dot{x}_2 = x_0x_1 - \beta x_2 + \gamma x_1 \sin(x_0 + x_2)$) at $\sigma = 0.01$. The three-dimensional state space is visualized via the x_0 - x_1 phase portrait. AUTOSINDY closely tracks parts of the true trajectory using a simple discovered equation (median complexity = 16).